TECHNICAL MEMORANDUM

181

Clouds and radiation

J-J. Morcrette, L. Illari, E. Klinker,
H. Le Treut, M.J. Miller,
P. Rasch and M. Tiedtke

Research Department

August 1991

European Centre for Medium-Range Weather Forecasts
Europäisches Zentrum für mittelfristige Wettervorhersage
Centre européen pour les prévisions météorologiques à moyen

Clouds and radiation

Document presented to the 19th Session of the Scientific Advisory Committee, 1991.

1. INTRODUCTION

From the beginning of operational forecasting at ECMWF, a fast and accurate parametrization of the cloud-radiation interactions has been among the most important features of the package of physical parametrizations. The 10-day forecast period is long enough for the effect of cumulative systematic errors in the radiation fluxes to influence the quality of the forecast significantly. This was verified on different occasions in the past (*Slingo and Ritter*, 1985) and more recently during experimentation and implementation of the new physical parametrizations (May 1989). These included a replacement of the radiation scheme. The revised radiation scheme helped maintain a more vigorous hydrological cycle and was largely responsible for curing the systematic decay of the model kinetic energy over a few days of integration (SAC paper on Radiation, 1989; on Systematic Errors, 1990).

The changes in the physical parametrizations of May 1989 have made the ECMWF model much more sensitive to cloud-radiation interactions over shorter timescales, especially through interactions with the convective processes in the tropics, and through the modulation of the energy available at the surface in the extratropics. Therefore, a proper diagnosis of the performance and deficiencies of the existing parametrizations is of primary importance. This paper reports on such a diagnosis and on some possible solutions.

Since the replacement of the radiation scheme in May 1989, no new data sets of clear-sky radiative fluxes (particularly of good quality observed fluxes) have been published that would allow a better assessment of the clear-sky fluxes in the ECMWF model, so this aspect of the parametrization will be addressed only briefly. Most of the new observational data sets (ERBE, SSM/I, Warren-Hahn's Surface Cloud Climatology, ISCCP) are more relevant to cloudy conditions, and section 2 presents comparisons of the model cloud and radiation fields with those observational data sets.

One main result of these comparisons is to emphasize the limitations of the present description of the cloud liquid water content by the diagnostic cloud scheme. Section 3 presents preliminary results obtained

ECMWF
Scientific Advisory Committee
19th Session

ECMWF/SAC/(91)6
Reading, 29 August 1991

Subject:	Clouds and radiation
Action required:	For discussion

1. INTRODUCTION

From the beginning of operational forecasting at ECMWF, a fast and accurate parametrization of the cloud-radiation interactions has been among the most important features of the package of physical parametrizations. The 10-day forecast period is long enough for the effect of cumulative systematic errors in the radiation fluxes to influence the quality of the forecast significantly. This was verified on different occasions in the past (*Slingo and Ritter*, 1985) and more recently during experimentation and implementation of the new physical parametrizations (May 1989). These included a replacement of the radiation scheme. The revised radiation scheme helped maintain a more vigorous hydrological cycle and was largely responsible for curing the systematic decay of the model kinetic energy over a few days of integration (SAC paper on Radiation, 1989; on Systematic Errors, 1990).

The changes in the physical parametrizations of May 1989 have made the ECMWF model much more sensitive to cloud-radiation interactions over shorter timescales, especially through interactions with the convective processes in the tropics, and through the modulation of the energy available at the surface in the extratropics. Therefore, a proper diagnosis of the performance and deficiencies of the existing parametrizations is of primary importance. This paper reports on such a diagnosis and on some possible solutions.

Since the replacement of the radiation scheme in May 1989, no new data sets of clear-sky radiative fluxes (particularly of good quality observed fluxes) have been published that would allow a better assessment of the clear-sky fluxes in the ECMWF model, so this aspect of the parametrization will be addressed only briefly. Most of the new observational data sets (ERBE, SSM/I, Warren-Hahn's Surface Cloud Climatology, ISCCP) are more relevant to cloudy conditions, and section 2 presents comparisons of the model cloud and radiation fields with those observational data sets.

One main result of these comparisons is to emphasize the limitations of the present description of the cloud liquid water content by the diagnostic cloud scheme. Section 3 presents preliminary results obtained

in research mode with prognostic cloud schemes which provide a more realistic representation of the 3-dimensional distribution of the cloud liquid water. All results presented in this section represent work in progress rather than solutions to problems.

The dependence of the parametrization package on the model horizontal and vertical resolution is important for future model development at ECMWF when the operational model will rely on the Integrated Forecast System (IFS, discussed in the SAC paper on Variational Analysis); amongst other capabilities the IFS can provide a variable grid over the globe. This topic is also relevant to the internal and external use of the ECMWF model for long integrations (seasonal at ECMWF for predictability research, or multi-year in outside institutions). In section 4, we present results of sensitivity studies which show the robustness of the ECMWF humidity and associated cloud and radiation fields when the horizontal resolution is changed.

In the final section, we discuss some further improvements that might be introduced in the ECMWF operational cloud-radiation parametrizations in the future, and we stress the need for more validation/verification of the model cloud-radiation products against observational data.

2. DIAGNOSTIC AND COMPARISONS WITH OBSERVATIONS

In this section we discuss the performance of the operational system in simulating the cloud and radiation fields. Section 2.1 discusses the cumulative impact of model changes in the last four years on various components of the energy budget. Section 2.2 discusses the validation of cloud and radiation processes through the use of a variety of observational data.

2.1 Impact of model changes on the energy budget

In this section we discuss the impact of model changes on various components of the energy budget. Results are displayed as departures from reference data sets such as ERBE or climatology, in order to clarify the evolution. The relevant model changes are summarized in Table 1.

2.2 Representation of cloud and radiation during the last four years

Recently, the first year (Feb.1985 to Jan.1986) of Earth Radiation Budget Experiment (ERBE) measurements has become available and we have used them to verify the model radiation fields at the top of the atmosphere (TOA) in the period 1987-1991. Figs. 1 to 4 present the differences between the model produced shortwave (SW) and longwave (LW) radiative fluxes over land and sea, between January 1987 and April 1991, and ERBE data. Although the present observations are not synchronous with the model simulations, the comparisons on a zonal mean basis are certainly useful for illustrating the impact of the recent changes in the model parametrizations on the radiation fields.

For surface radiative fluxes, no observational data set of sufficient quality is available and we rely on the climatology of surface fields over the ocean compiled at MPI by *Oberhuber* (1988). Figs. 5 and 6 present, over the ocean, the difference between the model simulated surface radiative fields in 1987-91 and climatological fields. Figs. 7 and 8 show the full model SW and LW fields over land in 1987-91; no well-established climatology is available for comparison.

Cycle	Date	Content
29	07/04/1987	Revision of the parametrization of surface processes
30	05/11/1988	Vertical diffusion above PBL is removed
31	22/11/1988	Change to initialization
32	**02/05/1989**	**New radiation scheme, replacement of Kuo by mass-flux convection,** revised gravity wave drag
33	04/07/1989	Bug-fix to spurious drizzle
34	16/08/1989	Change to initialization
35	16/05/1989	Physics recoded, **masking effect of vegetation on snow**
36	**05/06/1990**	**Evaporation of low wind speeds, introduction of non-precipitating convective clouds**
37	13/02/1991	Change to initialization
38	**09/04/1991**	**New surface albedo, maximum cloud overlap,** increased γ, revised vertical diffusion above PBL
39	**../09/1991**	**T-213-L31 model, maximum-random cloud overlap, fixed-liquid water mixing ratio for convective clouds**

Table 1: Changes in the forecast scheme since 1 January 1987. Those important for the representation of cloud-radiation interactions are printed in BOLD face.

As a reference data set for clouds, we have used the climatological global data set of total cloudiness from surface observations compiled by *Hahn et al.* (1982, 1984) and *Warren et al.* (1986, 1988). Results for 1987-91 are presented in Figs. 9 to 11 where we have subtracted from the model cloudiness the climatology for the period 1951-1981. Over this period, the climatological data are provided at a 5° horizontal resolution over both land and ocean. Since the observational data are from surface synoptic observations, this comparison is best aimed at verifying the total, low- and medium-level cloudiness because high clouds might be obscured by lower layers of clouds. Figs. 9 to 11 show the departure from

this climatology of the model clouds which are operationally archived as total, low- and medium-level cloudiness during the period 1987-91.

Comparisons with the observational datasets provided by Figs. 1-11 show the signature of the two main changes in the physical parametrizations.

Cycle 32

In May 1989 (model CY31 → model CY32), the increase in net solar radiation at the surface follows the replacement of the radiation scheme. The new scheme computes larger downward solar radiation due to a decrease in water vapour shortwave absorptivity. Over land, the increase in solar energy at the surface produces a warmer surface, larger sensible heat flux, and a warmer planetary boundary layer (PBL). Because the relative humidity threshold for diagnosing the low-level cloudiness was not retuned, the drier PBL became less cloudy. This caused the warm temperature bias in the lower troposphere observed during summer 1989 (as an excess of about 60 W m^2 around 50°N in June 1989 in Fig. 1). Over the ocean, the revision of the convection and radiation schemes weakened the temperature inversion at the top of the subtropical PBL. Therefore the amount of oceanic low-level cloudiness diagnosed from the strength of the inversion, generally located over the eastern parts of the oceanic basins, decreased. The new mass-flux scheme also suppressed the drizzle in the sub-tropics associated with the previous Kuo scheme and therefore contributed to the reduction of the low-level cloudiness over the western parts of the oceanic basins in the subtropics (increase of the positive errors poleward of 30° in Fig. 3, after May 1989). On the positive side, the more opaque high-level clouds in the new radiation scheme improved the longwave radiation budget at TOA in better agreement with the ERBE observations after May 1989 (Figs. 2 and 4, 15°N-15°S latitude band).

Cycle 36

In July 1990 (model CY35 → model CY36), the enhancement of the evaporation in case of low winds and the diagnosis of shallow convective clouds from the condensation rate certainly improved a number of features in the ECMWF model (*Beljaars and Miller*, 1990). However, with respect to cloud and radiation, the change can be seen as detrimental. The increased evaporation brought more moisture into the convergence zone with increased deep convection, and larger fractional cover of high clouds of slightly increased liquid water content. These high clouds appear too reflective in the shortwave range and too cold in the longwave range (Figs. 3 and 4, respectively, equatorward of 20°, after June 1990). In the subtropics, the shallow convective clouds compensate for the "inversion" stratiform clouds that had disappeared with CY32. However, the new clouds are usually formed in the western part of the oceanic basins, whereas the stratiform clouds are observed off the western coasts of the continents.

The surface fluxes also show the signature of these two changes. The May 1989 change increased the solar energy available at the surface by about 40 W m^{-2}, both because of the reduction in the amount of stratiform clouds (Fig. 10a) and the decreased water vapour SW absorbtivity in the new radiation scheme (see Figs. 5 and 7 around 40° in N.H. summer JJA'89 and S.H. summer D'89-J'90). In the longwave spectrum, the presence of the water vapour continuum absorption in the new scheme increased the downward flux at the surface in the intertropical area (see Fig. 6, equatorward of 15° after May 1989). The July 1990 changes decreased the SW radiation under the convective clouds of the ITCZ and the non-precipitating clouds of the subtropics (Fig. 10a), and similarly increased the downward LW radiation (Fig. 6, around 30°N).

Some of these changes have also put their mark on the behaviour of the model during the 10-day forecasts. The May 1989 changes have corrected for the systematic drop in the intensity of the hydrological cycle and of the kinetic energy, through a) a reduction of the spin-up (due to the mass-flux scheme) and b) a more steady Hadley circulation due to the increased LW clear-sky radiative cooling in the sub-tropics. This is clearly illustrated in Fig. 12 where the zonal means of the surface net solar radiation at day 1, 3, 5 and 10 are plotted for the 4 July months of 1987-1990. This improved stability of the fluxes over the full length of the forecasts is important to the users of ECMWF surface fields. However, the "interannual variability" due to the changes in the model is a major drawback for climatological use, as shown in Fig. 13 where the precipitation, surface and TOA radiation budgets and cloudiness over the TOGA/COARE area all display some signature of the model changes.

Cycle 38

In April 1991 (model CY37 → model CY38), a number of changes were introduced in the model, some of them directly related to the cloud-radiation parametrizations:

Albedo

A new mean annual surface albedo from *Dorman and Sellers* (1989) has replaced the mean annual surface albedo of *Geleyn and Preuss* (1983). The new albedo is the result of radiative transfer calculations of the plane albedo made by *Dorman and Sellers* (1989) for 13 different types of surfaces compiled from atlases of soil and vegetation types, and vegetation cover. It differs, in some areas substantially, from the previous model albedo derived by *Geleyn and Preuss* (1983) from polar-orbiter satellite channel measurements of reflectances. Such a derivation requires corrections to be applied to deal with the cloud screening, the atmospheric absorption, the conversion from a bi-directional reflectance to a plane albedo, from a narrow-band measurement to a total shortwave quantity, and a proper sampling of the diurnal variations of the correction factors. The main differences can be seen over the Sahara, where the new albedo is smaller (31 % instead of 35-48 %) and more homogeneous as the new climatology considers

one soil type only over this area. Smaller absolute differences are also seen over most of the continents with the new albedo generally larger, e.g., 12 % vs. 9 % over the Amazon basin, 11 % vs. 7 % over the U.S. Great Plains, 14 % vs. 10 % over Poland. These differences directly affect the net solar radiation available at the surface which is returned to the atmosphere as sensible and/or latent heat fluxes.

Radiation changes

A series of modifications were aimed at optimizing the cloud and radiation codes for use in a model with an increased vertical resolution:

- A cooling-to-space approximation to the longwave radiation transfer is applied to layers higher than 10 hPa (with no impact in the present configuration of the model, because of the absence of levels above 10 hPa).

- The overlapping of cloud layers was changed from a random overlap to a maximum overlap assumption to ensure a better treatment of the convective cloud towers. This change affects both the longwave and shortwave radiation schemes as well as the cloud scheme and includes a retuning of a number of parameters relevant to the diagnostic of the cloud distribution and optical properties (suppression of the wider base of the convective cloud, widening of the convective cloud, introduction of an omega- (vertical velocity) filter in the diagnostic of the middle-level cloudiness, increase of the proportionality factor γ relating the saturation mixing ratio to the cloud liquid water content (from 3 to 5 percent), tuning of the coefficients to allow inversion-capped low-level stratiform clouds to form under weaker temperature inversions).

Changing from a random to a maximum overlap assumption has the overall effect of decreasing the total cloudiness, and therefore of decreasing the radiative effects linked to the areal coverage by cloudiness. However, this effect can be partially compensated (especially in the shortwave range where the radiation transfer occurs in non-saturated conditions) by the increase in the vertically integrated optical thickness in the cloudy part of the atmosphere. With the random overlap assumption, the radiation code saw convective cloud towers as staggered layers whereas it handles them as true towers with the maximum overlap assumption. Everything else being equal, this change would allow more solar radiation to reach the surface (thus heating it), and more longwave radiation to escape to space (thus cooling the atmosphere). However, other modifications (particularly, the increase in low level cloudiness and the higher cloud liquid water content) compensate this direct impact and the overall effect of the cloud and radiation changes is a decrease in the solar radiation available at the surface and an otherwise small warming within the atmosphere in the tropics (Fig. 5, for April 91 in tropical regions).

Cycle 39

A set of physics changes has been developed as part of the preparation of the new high resolution model (T213/L31). The revised cloud scheme will allow the stratiform clouds to form in any number of layers instead of the three levels (high, medium, and low) in the previous version of the scheme. There will be a proper location of the anvil-cirrus cloud at the top of the convective tower, and another (slight) modification to use the random-maximum cloud overlap assumption first introduced by *Geleyn and Hollingsworth* (1979). Moreover, as a short-term measure before the implementation of a prognostic scheme for cloud liquid water, the cloud liquid water content (LWC) will be diagnosed separately for convective and condensation clouds. Convective clouds will be assigned a fixed liquid water mass mixing ratio of 1×10^{-4} kg/kg, while a proportionality factor γ of 5 % is kept for the other clouds. Finally, the mean effective radius assigned to the cloud droplets is allowed to vary with height from 10 microns at the surface to 45 microns at 100 hPa in an attempt to represent the variations of the droplet size within different types of clouds from relatively small droplets in stratocumulus clouds to large particles in cirrus clouds.

Future developments of the radiation and diagnostic cloud scheme

A version of the radiation scheme including the longwave absorption by CH_4, N_2O, and CFC-11 and -12 as well as the scattering and absorption effects of the climatological aerosols (*Tanré et al.*, 1984) is now available, mainly for long integrations. Whilst these new radiatively active constituents help decrease by a few W m^2 the OLR or the surface solar radiation in clear-sky conditions, their presence has not had any noticeable impact on the systematic errors or the quality of the 10-day research forecasts. Provision is also made to distinguish between ice and liquid water clouds using two sets of optical properties, and to introduce the first order effect of scattering by cloud droplets in the longwave window region by distinguishing between upward and downward cloud longwave emissivity as done by *Smith and Shi* (1991).

Feedback loops

This section has shown how much the cloud and radiation fields have been affected by the recent changes in the physical parametrizations. All of the changes in cloud-radiation interactions discussed above have also had a noticeable impact on the rest of the model through feedback loops with other physical processes.

For example, a decrease of low-level cloudiness over the summer continental masses (as happened during summer 1989) was further enhanced by the associated increase in surface radiative heating, the warming and decrease of the PBL relative humidity and the further decrease of the cloudiness (a positive feedback loop). In the process, the sensible heat flux increased, with a negative impact on the objective scores

through a spurious increase in the kinetic energy of the model. Over high terrain, the increased solar radiation available at the surface enhanced the effect of the elevated heat sources and contributed to the overestimation of the convective precipitation over the orography.

Another example of such a feedback loop is found in the tropics where an increase in low-level cloudiness (as in June 1990) is partly responsible for enhancing the evaporation through a change in radiative cooling within the cloud layer and a redistribution of that cooling within the well mixed layer. This in turn can increase the moisture available for the deep convective activity in the ITCZ, and strengthen the resulting Hadley circulation. As the subsidence in the descending branch is stronger, a stronger temperature inversion develops which leads to an increase in the inversion-capped low-level cloudiness.

In both cases, the interactions with other physical processes is much faster than the 10 to 20 day time-scale commonly accepted for radiative processes inasmuch as the clouds play a central role in these interactions. The modulation of the radiation fields by cloudiness occurs on the same time-scales as the moist processes to which they are linked. In view of the rapid interactions that can impact the quality of the model forecasts, it is therefore essential to validate/verify both the spatial and temporal behaviours of the cloud and radiation interactions not only over Europe but on a global scale. Comparisons with satellite observations play a major role in such a validation.

2.3 Diagnostics of model cloud and radiation fluxes with satellite data

Until recently, the validation of the cloudiness and of its radiative impact was made difficult by the absence of simultaneous and independent observations of radiation fluxes, cloud characteristics (e.g., cloud fractional cover, top temperature and pressure, optical thickness), and other parameters governing the radiation field (surface temperature, LW emissivity and SW albedo, water vapour distribution). From July 1987 (with the beginning of operational Special Sensor Microwave Imager SSM/I products) to February 1990 (with the termination of the scanner measurements on ERBS, the last satellite to carry a working ERBE payload), there is the potential availability of good quality measurements of cloud parameters in the various ISCCP (International Satellite Cloud Climatology Project) datasets, radiation fluxes (with the ERBE dataset) and vertically integrated water vapour and cloud water derived from the SSM/I observations. There is an on-going project of reassimilating (with a recent version of the ECMWF forecast system) a few months of meteorological data over that period starting with July 1987 in order to conduct a thorough validation of the cloud and radiation. As all observational datasets are not available yet to ECMWF, we discuss here preliminary results illustrating the potential use of these satellite observations.

Comparison with SSM/I observations

Klinker (1991) compared precipitable water content (PWC) from the model with PWC derived from SSM/I observations for July 1990. He found remarkable changes of the PWC in the first 5 days of the forecast indicating that the model has a general tendency to dry the subtropics and moisten large areas of the tropics where the deep convection occurs. The similarity of the PWC forecast change (Fig. 14b) to the PWC difference between the SSM/I analysis and the ECMWF analysis (Fig. 14a) suggests that the model has a tendency to approach a state which agrees more with the SSM/I analysis than with the ECMWF analysis, which at the time was based largely on NESDIS humidity retrievals over the ocean.

Comparison with ERBE data

Klinker (1991) also compared the greenhouse factor (ratio between the outgoing longwave radiation at the top of the atmosphere and the longwave radiation emitted from the surface, as done by *Raval and Ramanathan*, 1989) in the model for July 1990 with the one derived using ERBE measurements and NMC analysis of SST for July 1985. The general distribution of the greenhouse factor as a function of the temperature (Fig. 15a) agreed quite well with observations (Fig. 15b). However, the nonlinear increase for SST's higher than 295 K in the ITCZ was noticeably higher in the short-range forecast and even higher in the medium-range forecast suggesting an overestimation of the longwave cloud forcing.

A comparison of monthly mean modelled and observed radiation fields and cloud forcing for January 1986 by *Vesperini et al.* (1991) has given some insight about how the cloud-radiation interactions were handled in the cycle 34 version of the ECMWF model. It shows a good representation of the clouds in the storm tracks of the Northern Hemisphere; it also confirms the overestimation of both the shortwave and longwave impacts of clouds in the convective areas, the lack of low-level stratiform clouds over the cold waters of the eastern subtropical ocean basins, and the underestimation of the radiative impact of the clouds in the higher latitudes of the Southern Hemisphere.

The model changes leading to cycle 38 have been evaluated in a data assimilation experiment for a period of 5 days in July 1990. The radiation fluxes at TOA generated in the 6 hour forecast during the assimilation are compared here against ERBE data for July 1985. Though the time period of 5 days is relatively short, the differences between the model top solar radiation for cycle 36 and ERBE data (Fig. 16a) are similar to the differences for the full month of July 1990 (not shown). A positive bias over most areas of the Northern Hemisphere indicates a lack of cloud cover or deficiencies in the cloud optical properties. The increase of cloud liquid water for a given saturation mixing ratio in cycle 38 has reduced this bias over land and sea areas of the Northern Hemisphere (Fig. 16b). However, the general increase of cloud liquid water had a detrimental impact on the solar radiation fluxes in the tropics by increasing the negative bias even further. The changes in cycle 39 (fixed cloud liquid water for convective clouds)

retains most of the beneficial impact of cycle 38 in the Northern Hemisphere and reduced the bias in the tropics to the level of the cycle 36 bias (Fig. 16c).

The increase of low-level cloudiness with cycle 38, especially along the western coasts of the continents brought the net solar radiation closer to observed values. However, the spurious low-level cloud cover in summer over the Mediterranean Sea and in the same latitude range over the East China Sea has been further increased resulting in a larger bias in the solar radiation for cycles 38 and 39 over these areas.

The reduction of the positive bias in the Northern Hemisphere between cycle 36 and cycle 38 must be partially attributed to an increase of the surface albedo. The positive radiation bias over Sahara in cycles 38 and 39 suggest that the albedo reduction over this desert area might have been too large.

Compared to the solar radiation, the impact of cycles 38 and 39 model changes on the OLR is relatively small (Fig. 17). The overestimation of the OLR over the summer continental areas is slightly reduced with cycle 39.

Comparison with ISCCP-B3 data

The verification of the cloudiness and its radiative effects on short time scales, which would be even more relevant for understanding the interactions between, say, the convective processes, the evolution of the associated cloud field, and the radiative processes, is particularly difficult. Even one of the most advanced retrieval scheme to date (the ISCCP cloud algorithm, *Rossow et al.*, 1988) has to rely on some time compositing to retrieve successfully the clear-sky radiances which serve as background over which an observed instantaneous radiance will be classified as clear-sky or cloudy. As illustrated for example by *Morcrette* (1991c), such a compositing procedure can introduce large uncertainties in the retrieved cloud cover and subsequent derived parameters. On short time scales (hours to a few days), very useful information is obtained from a more direct approach, the"model-to-satellite" method (*Morcrette*, 1991b) where radiances as similar as possible to the satellite observations are produced from the model variables.

Figs. 18 to 20 compare over a number of limited areas [$(10.125°)^2$, i.e. 9 x 9 T106 grids] the evolution histograms of the longwave window brightness temperature EH(T_B) (*Morcrette*, 1991b) as observed by METEOSAT and modelled by the ECMWF for a 4-day period in July 1983. Results are shown for the observed T_B degraded to the model T106 resolution and for simulations with the cycle 31 and 36 of the ECMWF model. Fig. 18 corresponds to the observed EH(T_B) over four limited areas, namely a) the Cape Verde Islands area where low-level stratiform clouds are prevailing, b) the Niger-Nigeria area where the dominant feature is the strong diurnal cycle of both the surface temperature and the convective cloudiness, c) the Sierra Leone Basin with quasi-permanent convection over the ocean, and d) the Gough Island area

displaying the signature of passing frontal systems. Fig. 19 shows the EH(T_B) simulated with the CY31 physics, with very few scattered clouds over the Cape Verde Island, and too transparent clouds (especially the high-level ones) over the other three areas. The Sierra Leone Basin area also shows a gap in the distribution of the T_B around 270 K (about 500 hPa) indicating the absence of cloud tops in that temperature range. Fig. 20 presents results with the CY36 model. More cloudiness is now observed over the Cape Verde Islands area but not of the stratiform type, and the three other areas now display the signature of much more radiatively active high-level cloudiness.

This section presented only a few preliminary results and illustrated the improved knowledge of the atmosphere and of the surface-cloud-radiation interactions that can be gained from satellite observations. These observations will therefore be extensively used in the future to improve the parametrizations.

2.4 Discussion

As seen from the history of ECMWF model cloud and radiation fields, any model change that impacts the moisture and temperature distributions may significantly modify the clouds and associated radiation fields. Satellite observations provide a wealth of information directly relevant for validating the clouds and radiation generated by a model if the spatial and temporal variability of these model outputs is studied as well as the more usual time averages. Comparisons with satellite observations also show the limitations of the diagnostic approach to the cloud formulation, particularly regarding the cloud water content. Only prognostic schemes, which allow for a consistent treatment of the condensation, cloud, precipitation and evaporation water, offer a viable way to physically link the radiative and the moist processes in the model.

3. PRELIMINARY RESULTS WITH PROGNOSTIC SCHEMES

The main conclusion from the previous comparisons with observations is that cloudiness and associated radiation fields show a distinct impact of any changes in the model moisture field. We also feel that the limitations of diagnostic cloud schemes justify an effort on developing prognostic cloud schemes.

New schemes have recently been tested within the ECMWF model, which allow for a more realistic treatment of the water content of clouds. Any change in the liquid water within the clouds impact the radiation fields. *Tiedtke* (1991) has proposed an extension of the mass-flux scheme (*Tiedtke*, 1989) with prognostic equations for both the convective cloud cover and convective cloud liquid water content as well as a unified scheme for convective and non-convective clouds. *Le Treut* (1991) has tested the scheme originally developed for the model of Laboratoire de Meteorologie Dynamique (*Le Treut and Li*, 1991), with a prognostic equation for the stratiform clouds. In the following, we compare cloudiness and related radiation fields obtained with the operational diagnostic cloud scheme, as originally designed by *Slingo*

(1987) (CY36) and as recently revised (CY39), with these two new prognostic schemes (SC and UN). Table 2 below summarizes the characteristics of the four T63 simulations of July 1987 discussed hereafter.

Experiment	Convective cloud	Stratiform cloud	γ
CY36	Operational	Operational	0.03 (all)
CY39	Operational	Operational	0.05 (SC) $1x10^{-4}$kg/kg (CC)
SC	Operational	Le Treut (1989)	$1x10^{-4}$ kg/kg (CC)
Unified	Tiedtke (1991)	New	N/A

Table 2: Characteristics of the four T63 simulations of July 1987

3.1 The Le Treut and Li prognostic scheme for cloud condensed water content in stratiform clouds

The scheme, originally developed for a climate model (*Le Treut and Li*, 1991), includes a new prognostic equation for total water and a diagnostic relationship from which cloud water and cloud fraction are determined assuming that the cloud population depends statistically on the large scale moisture field (q), the vertical velocity (ω) and the Richardson number (Ri), through a moisture variance

$$(\Delta q_t)^2 \sim \left(\sigma_w \frac{\partial q}{\partial z} \Delta t\right)^2$$

where $\sigma_w = \dfrac{a + b|\omega|}{\ln (1 + \max (0, Ri))}$

From the knowledge of Δq, cloud fraction and cloud water content are determined. Microphysics are parametrized following *Kessler* (1969), but a distinction has been made between warm and cold clouds. A more detailed description of the scheme together with preliminary results can be found in *Le Treut* (1989).

The scheme has been tested in some long integrations (at T42 and T63) and in a few T106-10 days forecasts. Results presented hereafter are from a version of the scheme which has been coupled with the radiation and the diffusion schemes. However, there is no coupling with the convection scheme. Convective cloud cover and liquid water amount are still represented by the operational diagnostic scheme (CY39 version). The coupling with the vertical diffusion scheme assumes that in the test of buoyancy in presence of cloudiness (in the computation of the Richardson number), the air parcels follow the moist rather than the dry adiabat. This coupling has proved to be particularly relevant to the representation of

boundary layer clouds (Fig. 21). Stratocumulus decks, off the coast of California and Angola, are better represented in the SC experiment. They are nearly absent in the control CY36 experiment.

3.2 A unified fully prognostic scheme for convective and non-convective clouds

The unified scheme for convective and non-convective clouds is an extension of a prognostic scheme originally proposed for cumulus cloud fields (*Tiedtke*, 1991). In addition to the formation and dissipation of clouds in connection with cumulus convection, it considers the formation of stratiform clouds by condensation. Thus the following processes are now considered:

cloud formation

- detrainment of cloud air from cumulus updrafts (*Tiedtke*, 1991)
- condensation due to large-scale ascent and diabatic cooling in terms of

$$\frac{dq_s(p,T)}{dt} = -\omega \frac{dq_s}{dp} + \frac{dq_s}{dT}\left(\frac{\partial T}{\partial t}\right)_{diab}$$

cloud dissipation

- evaporation due to large-scale subsidence and diabatic heating (formally the same as for condensation);
- precipitation processes (*Sundqvist*, 1988);
- turbulent mixing of cloud air and unsaturated environmental air proportional to the saturation deficit of environmental air.

It should be noted that this scheme uses two new prognostic equations and, in contrast to most other schemes, predicts cloud water content **and** cloud area, which is usually diagnosed. Uncertainties in the parametrization exist primarily through tunable parameters for precipitation processes, the turbulent diffusion coefficient and the assumption for the critical humidity above which stratiform clouds are assumed to form, which at present is between 90 % and 100 % depending on height above ground. Validation of the scheme indicates that boundary layer clouds are not represented adequately and an extension of the scheme may be necessary by linking it to the boundary layer scheme which includes moist processes.

3.3 Comparisons of cloud parameters

Figs. 22 to 25 present the latitudinal/height cross-sections of the zonally averaged cloud fractions on top panels and of the cloud liquid water content on bottom panels given by the four simulations. Fig. 22 corresponds to the control CY36 model, Fig. 23 to the revised diagnostic formulation of CY39, Fig. 24

to the stratiform clouds (SC) produced by Le Treut's scheme and Fig. 25 to the results of the fully prognostic scheme (UN).

The main features of the observed cloud cover distribution are the convective "towers" in the deep tropics topped by some anvil-type clouds, the relative minima in the subtropics and the higher values of the cloud cover at middle-to-high latitudes. Those features are present in all simulations.

In the CY36 simulation (Fig. 22), the diagnosed convective clouds in the tropics display a maximum at low levels, corresponding to the bottom part of the L-shape distribution assumed for the convective clouds. In the operational CY36 scheme, the convective clouds are diagnosed from the accumulated convective precipitation rate and occupy all layers between the base and the top of the column undergoing convective adjustment. However, a weighting factor of 0.25 is applied to the convective cloud fractional cover in all layers except the lowermost, in an attempt to represent the shallow convective clouds (this is referred to as the L-shaped convective clouds). In the CY39 simulation (Fig. 23), allowing for more than one cloud layer within each of the three atmospheric slices (low, medium, and high) increases the overall cloudiness, especially at the top of the tropical convective tower, and is, in this respect, most similar to the UN simulated cloud cover.

The operational CY36 cloud scheme simply diagnoses the cloud liquid water content (LWC) as a given fraction of the saturation mixing ratio of water vapour. As seen in Fig. 22, this leads to a cloud liquid water path (LWP) varying as a strong function of the local temperature, with maximum value in the lower layers of the tropics and rapid decrease in higher layers or/and at higher latitudes. In CY39, the increase in the proportionality factor γ for the stratiform clouds and the fixed mass mixing ratio for the convective cloud liquid water gives a very different distribution of the cloud liquid water amount. In particular, it gives higher LWP over the whole vertical extent of the deep convective clouds as also obtained in the UN simulation. However, the LWP derived for the stratiform clouds has its maximum values close to the surface and cannot represent the relative maximum of LWP located higher up in both the SC and UN simulations.

As previously discussed, the CY36 simulation displays a large cover by convective clouds at low levels as a result of the L-shape assumed for convective cloud tower, a feature which was suppressed with CY38. The new prognostic scheme (UN) for convective clouds does not give any such maximum either.

The new prognostic schemes both give a very different (and intuitively) more realistic picture of the distribution of the liquid water content, with maximum values for the clouds poleward of 45°, at height well above the PBL. These features are produced by both prognostic schemes and to some extent by the

revised diagnostic scheme. Both prognostic schemes are successful at describing extratropical clouds together with some tropical anvil clouds. Cloud cover and cloud liquid water amount (Fig. 24 and 25, a and b) in the upper troposphere are increased when compared to control CY36 experiments (Fig. 22 a and b).

The geographical distribution of the vertically integrated cloud liquid water derived over the ocean from SSM/I microwave measurements are shown in Fig. 26, together with similar quantities derived from the experiments. The CY36 simulation clearly overestimates the cloud liquid water in the tropics, while other simulations show reasonable agreement with observation.

The drastic changes in the three-dimensional distribution of the cloud LWC between CY36 and the other experiments is of relevance for the associated radiative fluxes. Fig. 27 presents the zonally averaged shortwave and longwave radiative fluxes at TOA and at the surface from these four experiments which used the same radiation scheme and cloud optical properties. ERBE measurements for July 1985 are added to the TOA fluxes for comparison. The larger improvement is seen in the shortwave fluxes in the tropical region, where the agreement between UN and ERBE fluxes becomes good. At higher latitudes, both UN and SC fluxes get closer to ERBE fluxes but the discrepancy at 50°N is still 20 W m^{-2}. North of 60°N, none of the simulations is in agreement with the measurements, suggesting a lack of cloudiness and/or too small LWP. In the longwave, the prognostic schemes produce clouds which allow more radiation to escape to space. Although the fractional cover by anvil-type clouds is not decreased and the liquid water content is in fact slightly increased by the UN scheme, this larger loss of energy to space is due to the disappearance of the low-level maximum of LWC. Comparisons with ERBE OLR show that the maximum in the clear-sky sub-tropics is overestimated by 20 W m^{-2}, a feature partly due to the absence of absorption by aerosols and trace gases (N_2O, CH_4) in this version of the radiation scheme.

A large impact is also seen on the radiation fluxes at the surface (bottom panels in Fig. 27). The shortwave fluxes increase by up to 50 W m^{-2} under the prognosed convective clouds due to the suppression of the low-level maximum of LWC. At higher latitudes, the larger cloud LWC produced by the UN scheme contributes to decreasing the solar radiation available at the surface. In the longwave range, the shift to higher levels of the maximum LWC decreases the downward longwave flux at the surface by at least 10 W m^{-2}, with maximum changes of 30 W m^{-2} under the convective clouds.

3.4 Discussion

As noted earlier, the importance of cloud-radiation interactions and the limitations of doagnostic cloud schemes justify the development of prognostic cloud schemes. We have compared the performance of

several diagnostic and prognostic schemes. The results from the prognostic schemes show real promise and justify further work.

4. SENSITIVITY TO MODEL HORIZONTAL RESOLUTION

A recent paper by *Kiehl and Williamson* (1991) reports a study carried out with the NCAR Community Climate Model which shows the model cloudiness to be highly dependent on the model horizontal resolution. In their experiments which encompass resolutions from R15 to T106, the globally averaged total cloudiness decreases from 0.47 at R15 to 0.26 at T106 using the original cloud scheme of *Ramanathan and Dickinson* (1981) and from 0.54 at T21 to 0.42 at T63 when including a Slingo-type diagnostic cloud scheme.

Similar experiments have been run with the ECMWF model for July 1987 for the 4 resolutions T21, T42, T63, and T106, using either the operational mass-flux scheme to deal with the convective processes, or the pre-May'89 Kuo scheme with the shallow convective part of the scheme either active or inactive, or the Betts-Miller adjustment scheme, or in its simplest configuration, without any deep convection parametrization. As can be seen from Fig. 28 which presents the different components of the globally averaged cloudiness, the moisture field and therefore the cloudiness is a very stable feature in the ECMWF model in 31-day simulations. Zonal means of the total cloudiness for the different model configurations (not shown) show that the largest variations are mainly seen:

i) for low-level cloudiness at high latitudes, as at T21 the negative humidity fixer creates areas of high relative humidity over orography (Greenland and Antarctica) whereas it is much less active at higher horizontal resolutions;

ii) for high-level cloudiness, larger at T21 over the subtropics, as a result of a wider and less intense convergence zone at lower resolution.

However, if the three-dimensional distribution of cloudiness appears quite stable when changing the resolution, large differences can be seen in the day-to-day variability of the cloudiness and associated radiative fields, as illustrated in Figs. 29 to 31 which show for three latitude bands the Hovmöller diagrams of the longwave cloud forcing in July 1987 as described by the CY36 version model at the four horizontal resolutions.

5. CONCLUSIONS

From the first operational forecasts in 1978, the ECMWF model has included a parametrization of cloud and radiation interactions including interactive clouds inasmuch as the cloud fraction and liquid water

content are linked to the model humidity and temperature fields. Since 1985, the cloudiness has also been a (experimental) model product distributed to the Member States on which they have come to rely more and more. Over the last few years, the cloud cover has therefore been operationally verified against synoptic observations, almost exclusively over Europe. However, the comparisons with observations of section 2 show that recent changes in the physics package have had large systematic changes in cloudiness mostly in the tropics. It is therefore important that future changes in the model likely to affect the cloudiness be assessed with equal consideration to the cloudiness outside of European area.

As judged by a recent survey of the existing radiation parametrizations for GCMs (*ICRCCM*, 1991), the ECMWF radiation package is certainly state-of-the-art with regards to clear-sky radiation fluxes. However, the validation carried out when the scheme was developed mostly included comparison with results of more detailed computations by either line-by-line or narrow-band models first calibrated on line-by-line model results. Verification of the absorption coefficients in the clear-sky parametrizations will therefore be performed against the latest release of the compilation of spectroscopic parameters (AFGL'91). An effort will be pursued to carry out more validation with observational datasets, as, for example, done recently by *Bréon et al.* (1991) with the longwave part of the ECMWF radiation scheme.

The new surface albedo appears more realistic (except over Sahara where it might be too low), but needs to be checked against recent estimations of albedo or net solar radiation from satellite measurements. The climatology by *Dorman and Sellers* (1989) offers prospects for the future: Monthly albedo are available which incorporates the seasonal cycle of the vegetation, as well as monthly means of the vegetation resistance and roughness essentially consistent with the shortwave albedo as they are all relying on the same soil and vegetation type distributions. A major effort will be devoted to verification of the surface radiation fields in the future.

The preliminary results obtained with new research cloud schemes (section 3) show that the liquid water content assigned to the clouds up to now by the present operational diagnostic scheme is far from realistic. The new results cast doubt on any attempt at verifying the three-dimensional distribution of radiation fields. In fact, a correct vertical distribution of the cloud liquid water is, with the fractional cover, paramount to the proper determination of the radiative fluxes, particularly in the longwave range. Unfortunately, we are still very far of being able to verify this quantity from observations, as even the new SSM/I measurements give access to only vertically integrated cloud liquid water.

Until the new prognostic schemes produce model distributions of cloud liquid water close to the actual distribution of cloud liquid water, there may be little point in addressing potential improvements in handling the effects of clouds on the radiation fields (e.g., improving the cloud optical properties through

differentiating various types of cloudiness, or including the effect of scattering by cloud droplets in the longwave) and even more so as long as the model includes a diagnostic cloud scheme. The gross unrealism of the cloud LWC may have been less of a problem before May 1989 as the previous radiation scheme was much less sensitive to the clouds (due to the model cloud assumed for the off-line Mie computations of its absorption and scattering coefficients; *Morcrette*, 1990, 1991a).

One outcome of the comparisons with the observations of section 2 and of the preliminary studies with prognostic cloud schemes (section 3) is the high sensitivity of the radiation fluxes at TOA and at the surface to the details of the cloud fields. In that respect, it is clear that the validation of the cloud and radiation fields is a continuing process, that validation cannot be done once and for all, and the adequacy of a given parametrization has to be challenged every time a new observational data set becomes available.

Up to recently, the only validation possible was that of radiation fluxes at the top of the atmosphere. The ISCCP and surface cloud climatology data sets allow for validation of some of the cloud characteristics (mostly cloud fractional cover but also cloud top height and temperature and reflectance). The overall radiative impact of the cloudiness (the SW and LW cloud forcings) can be checked using the ERBE data, in particular the derived clear-sky fluxes. Unfortunately, the radiative fluxes at the surface and the radiative heating/cooling rates cannot be validated due to the lack of observational data sets. ECMWF should become more closely connected with the programs of in situ observations to gain quicker access to the experimental measurements (such as those already obtained during FIRE-1 on cirriform and stratiform clouds, or those to be observed in the near future during TOGA/COARE, FIRE-2 or EUCREX or as part of the U.S. DOE Atmospheric Radiation Program). Inasmuch as the 3-dimensional distribution of cloud fraction and cloud liquid water content are very important parameters for understanding the role of the clouds in their interactions with the rest of the model, those quantities should be operationally archived instead of the less meaningful four cloud fractions we presently keep.

With the potential implementation of a prognostic cloud scheme in the ECMWF forecast model in the not too distant future, it is crucial that the possibility of an operational analysis of cloud parameters be studied in detail. Different approaches are possible using either direct satellite-observed cloudy radiances in the longwave and/or microwave ranges of the spectrum or retrieved cloud liquid water from SSM/I (and cloud cover from AVHRR as recently proposed by NOAA/NESDIS).

Finally the history of radiation fluxes in the ECMWF model shows that large changes occurred in May 1989 and July 1990, and that further large changes can be expected if a prognostic cloud scheme becomes

operational. Thus the archived ECMWF operational model radiation fluxes cannot be used as a representative climatology of radiation by the outside research community.

REFERENCES

Beljaars, A., and M. Miller, 1990: A note concerning the evaporation from the tropical oceans - Sensitivity of the ECMWF model to the transfer coefficient of moisture at low wind speeds. ECMWF Technical Memorandum No. 170.

Bréon, F.-M., R. Frouin, and C. Gautier, 1991: Downwelling longwave irradiance at the ocean surface: An assessment of in situ measurements and parameterizations. J.Appl.Meteor., 30, 17-31.

Dorman, J.L., and P.J. Sellers, 1989: A global climatology of albedo, roughness length and stomatal resistance for atmospheric general circulation models as represented by the simple biosphere model (SiB). J.Appl.Meteor., 28, 833-855.

Geleyn, J.-F., and A. Hollingsworth, 1979: An economical analytical method for the computation of the interaction between scattering and line absorption of radiation. Beitr.Phys.Atmosph., 52, 1-16.

Geleyn, J.-F., and H.-J. Preuss, 1983: A new data set of satellite-derived surface albedo values for operational use at ECMWF. Arch.Meteor.Geophys.Bioclim., 32, Ser.A, 353-359.

Hahn, C.J., S.G. Warren, J. London, R.M. Chervin, and R. Jenne, 1982, 1984: Atlas of Simultaneous Occurrence of Different Cloud Types over the Ocean/Land. NCAR Technical Note TN-201+STR / TN-241+STR, Boulder, Co., 212 pp. / 216 pp.

ICRCCM, 1991: The InterComparison of Radiation Codes in Climate Models. J.Geophys.Res., 86D, 8921-9158 [Special section No.D5, 16 papers].

Kiehl, J.T., and D.L. Williamson, 1991: Dependence of cloud amount on horizontal resolution in the National Center for Atmospheric Research Community Climate Model. J.Geophys.Res., 96D, 10955-10980.

Klinker, E., 1991: Use of satellite data to validate the hydrological cycle of the ECMWF model. ECMWF/WCRP Workshop on Clouds, Radiation and the Hydrological Cycle, ECMWF, Reading, U.K., 12-15 November 1990, 179-198.

Le Treut, H., 1989: First studies with a prognostic cloud generation scheme. ECMWF Technical Memorandum No. 155, 32 pp.

Le Treut, H., 1991: Sensitivity and validation studies with a prognostic cloud generation model. ECMWF/WCRP Workshop on Clouds, Radiation and the Hydrological Cycle, ECMWF, Reading, U.K., 12-15 November 1990, 223-240.

Le Treut, H., and Z.-X. Li, 1991: Sensitivity of an atmospheric general circulation model to prescribed SST changes: Feedback effects associated with the simulation of cloud optical properties. Climate Dynamics, 5, 175-187.

Morcrette, J.-J., 1990: Impact of changes to the radiation transfer parameterizations plus cloud optical properties in the ECMWF model. Mon.Wea.Rev., 118, 847-873.

Morcrette, J.-J., 1991a: Radiation and cloud radiative properties in the ECMWF operational weather forecast model. J.Geophys.Res., 96D, 9121-9132.

Morcrette, J.-J., 1991b: Evaluation of model-generated cloudiness: Satellite observed and model-generated diurnal variability of brightness temperature. Mon.Wea.Rev., 119, 1205-1224.

Morcrette, J.-J., 1991c: Diagnostics of cloud-radiation interactions using model-simulated Meteosat brightness temperatures. ECMWF/WCRP Workshop on Clouds, Radiation and the Hydrological Cycle, ECMWF, Reading, U.K., 12-15 November 1990, 295-312.

Oberhuber, J.M., 1988: An atlas based on the COADS dataset: The budget of heat, buoyancy and turbulent kinetic energy at the surface of the global ocean. Max-Planck-Institute for Meteorology Report No.15, Hamburg 13, F.R.G., 196 pp.

Raval, A., and V. Ramanathan, 1989: Observational determination of the greenhouse effect. Nature, 342, 758-761.

Rossow, W.B., E. Kinsella, A. Wolf, and L. Garder, 1987: International Satellite Cloud Climatology Project (ISCCP): Description of Reduced Resolution Radiance Data. July 1985 (revised July 1987). WMO/TD-No.58, World Meteorological Organization, Geneva, 143 pp.

Rossow, W.B., L.C. Garder, P.J. Lu, and A.W. Walker, 1988: International Satellite Cloud Climatology Project (ISCCP): Documentation of Cloud Data. WMO/TD-No.266, World Meteorological Organization, Geneva, 78 pp. + 2 appendices.

Slingo, J.M., 1987: The development and verification of a cloud prediction scheme for the ECMWF model. Quart.J.Roy.Meteor.Soc., 113, 899-928.

Slingo, J.M., and B. Ritter, 1985: Cloud prediction in the ECMWF model. ECMWF Tech. Report No. 46, ECMWF, Reading, U.K., 46 pp.

Smith, E.A., and Lei Shi, 1991: Surface forcing of the infrared cooling profile over the Tibetan Plateau. J.Atmos.Sci., submitted.

Sundqvist, H., 1988: Parameterization of condensation and associated clouds in models for weather prediction and general circulation simulation. In: Physically-Based Modelling and Simulations of Climate and Climatic Change, 433-461.

Tanré, D., J.-F. Geleyn, and J.M. Slingo, 1984: First results of the introduction of an advanced aerosol-radiation interaction in the ECMWF low resolution global model, in Aerosols and Their Climatic Effects, H.E. Gerber and A. Deepak, eds., A. Deepak Publish., Hampton, Va., 133-177.

Tiedtke, M., 1989: A comprehensive mass-flux scheme for cumulus parameterization in large-scale models. Mon.Wea.Rev., 4117, 1779-1800.

Tiedtke, M., 1991: Aspects of cumulus parametrization. ECMWF Seminar on Tropical Extra-Tropical Interactions, ECMWF, Reading, 10-14 September 1990, 441-466.

Vesperini, M., J.-J. Morcrette, and Y. Fouquart, 1991: Simulation of cloud radiative forcing with the ECMWF model. ECMWF/WCRP Workshop on Clouds, Radiation and the Hydrological Cycle, ECMWF, Reading, U.K., 12-15 November 1990. Dyn.Atmos.Oceans. to appear.

Warren, S.G., C.J. Hahn, J. London, R.M. Chervin, and R. Jenne, 1986 / 1988: Global Distribution of Total Cloud Cover and Cloud Type Amounts over Land. / the Ocean NCAR Technical Note TN-273+STR / TN-273+STR, Boulder, CO.

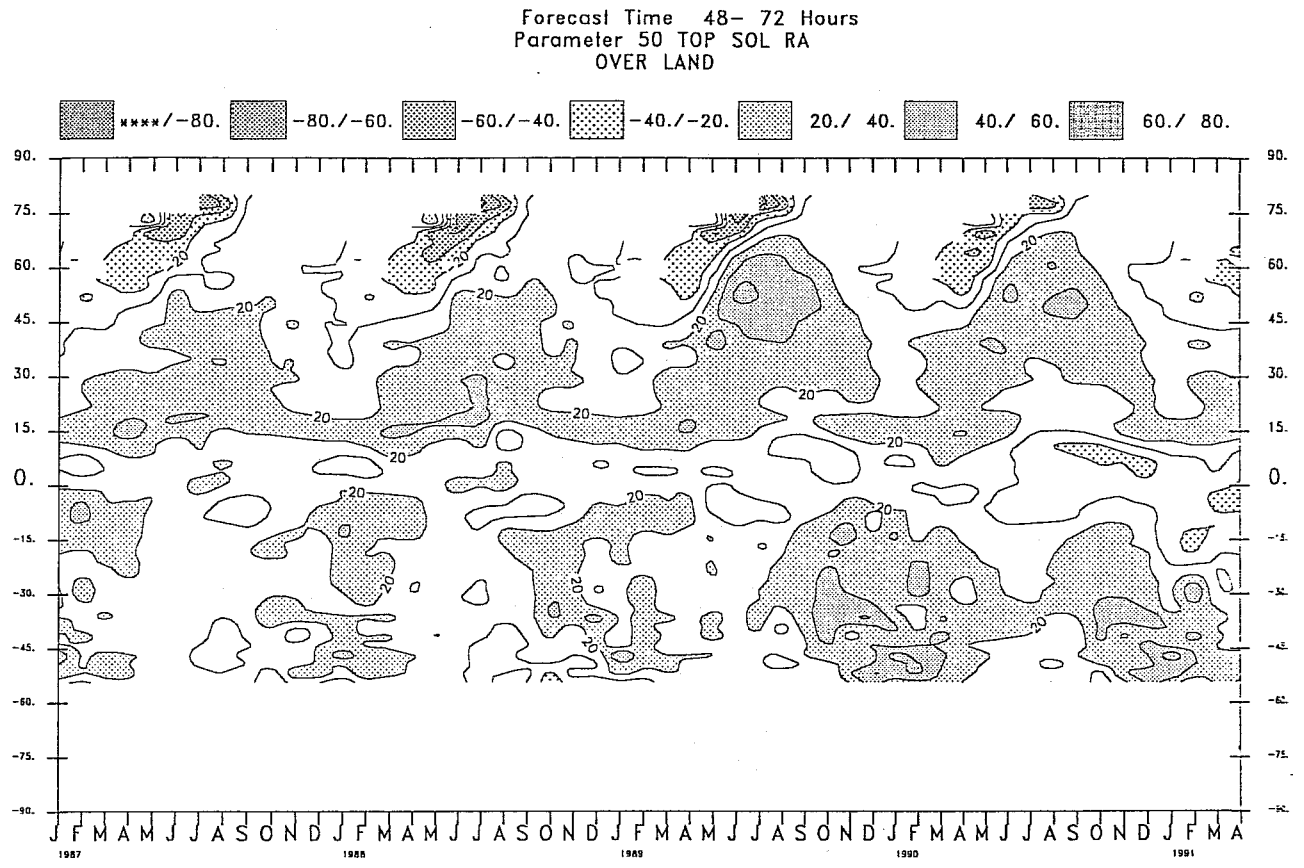

Fig. 1 Time evolution of the difference with ERBE observations of the net shortwave radiation at the top of the atmosphere zonally averaged over land points. Units are W m^{-2}

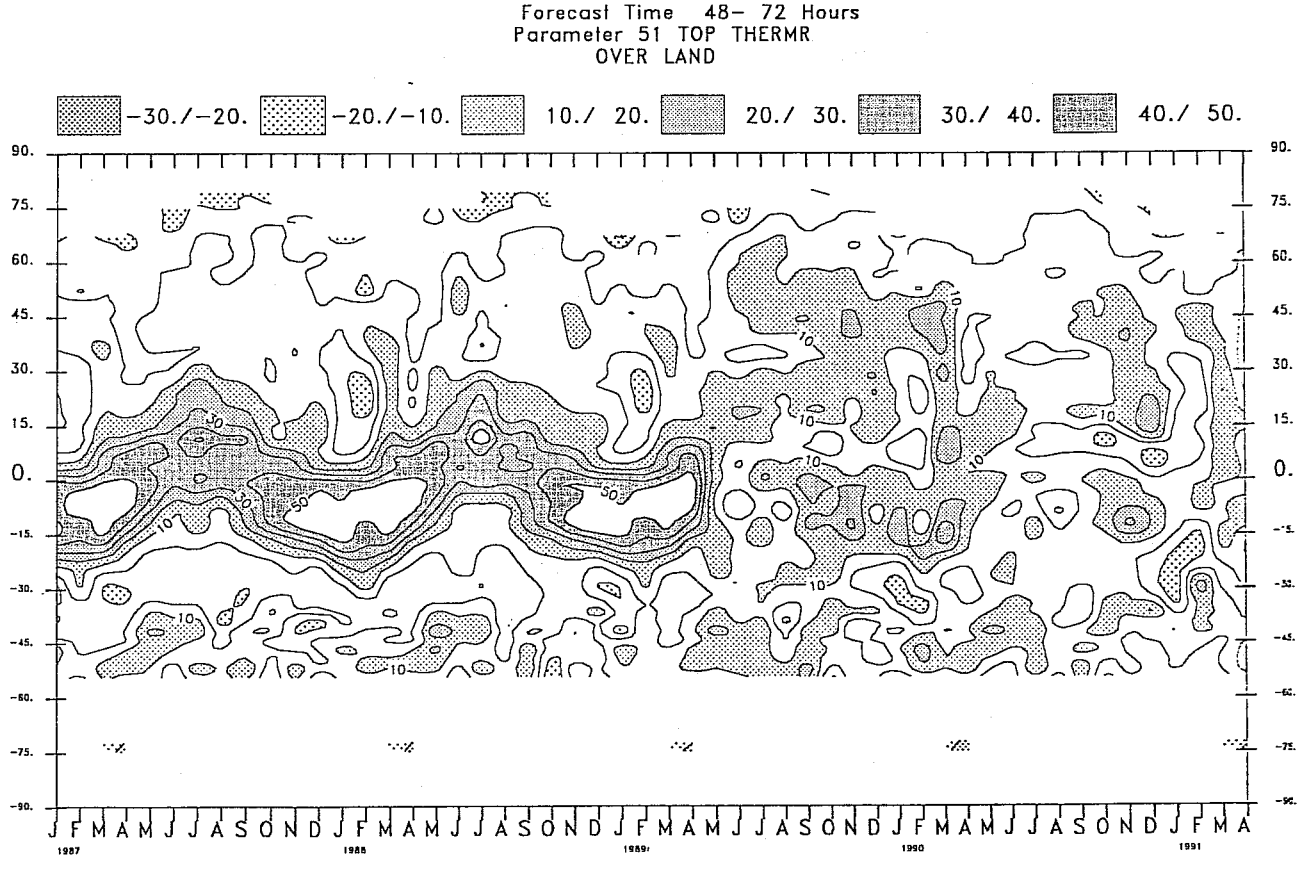

Fig. 2 Time evolution of the difference with ERBE observations of the model outgoing longwave radiation at the top of the atmosphere zonally averaged over land. Units are W m^{-2}.

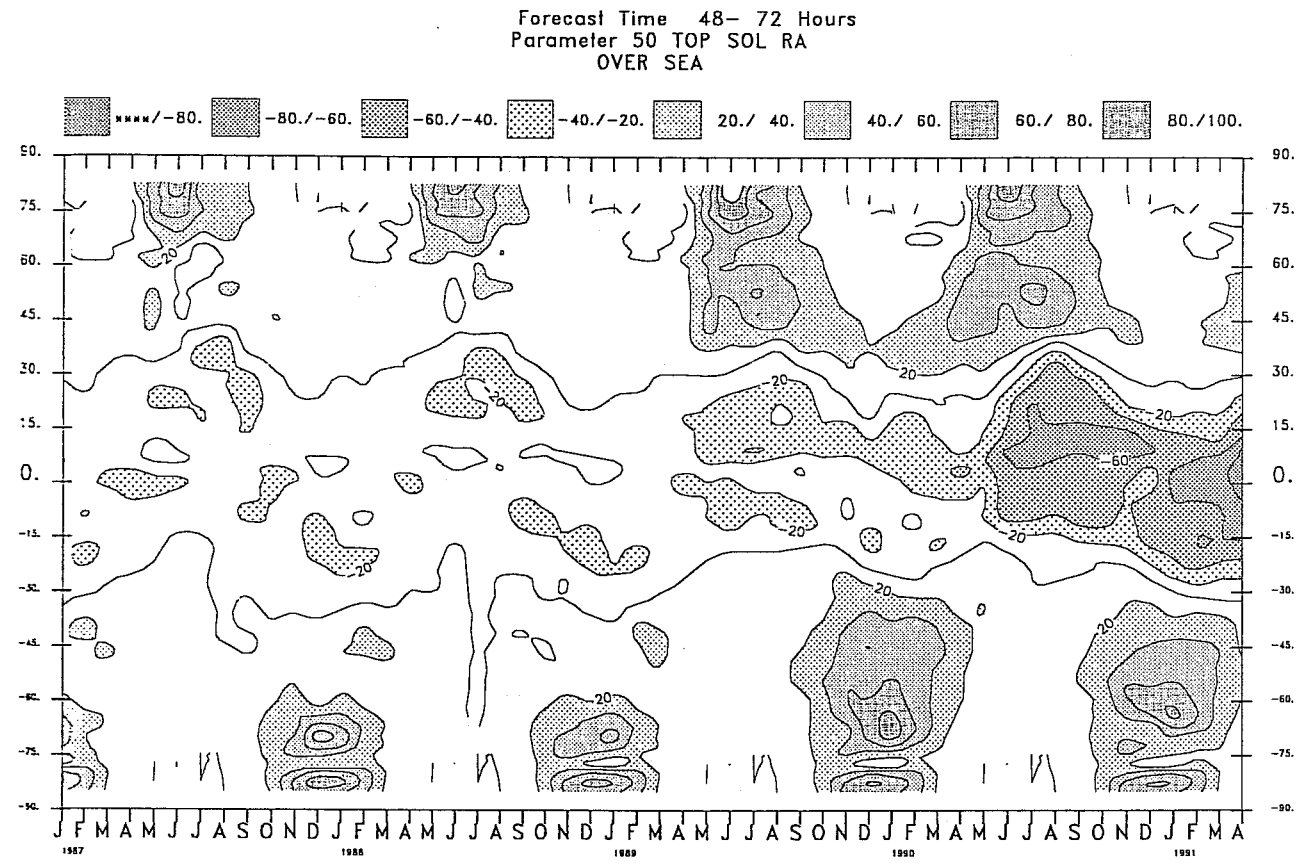

Fig. 3 As in Fig.1, but over the ocean.

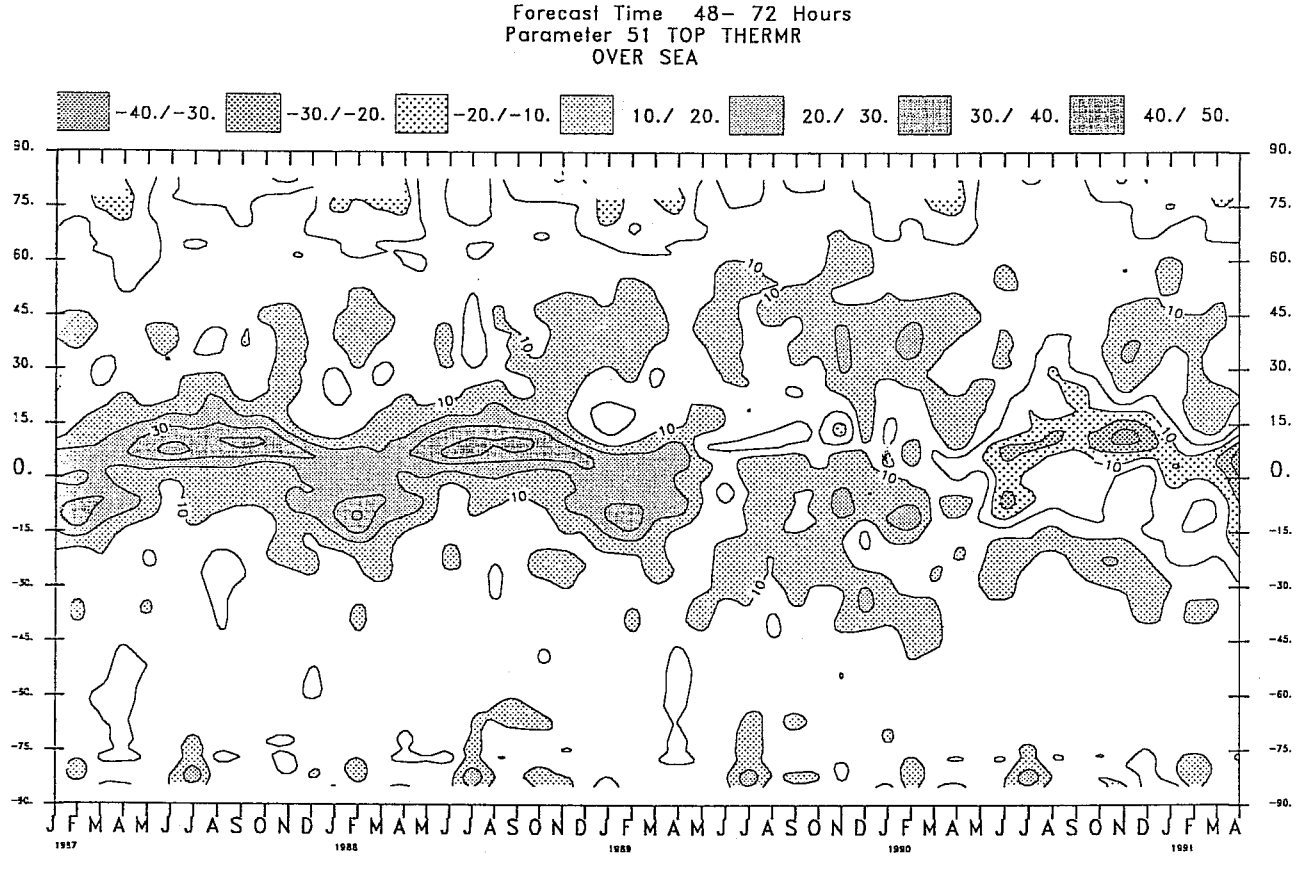

Fig. 4 As in Fig.2, but over the ocean.

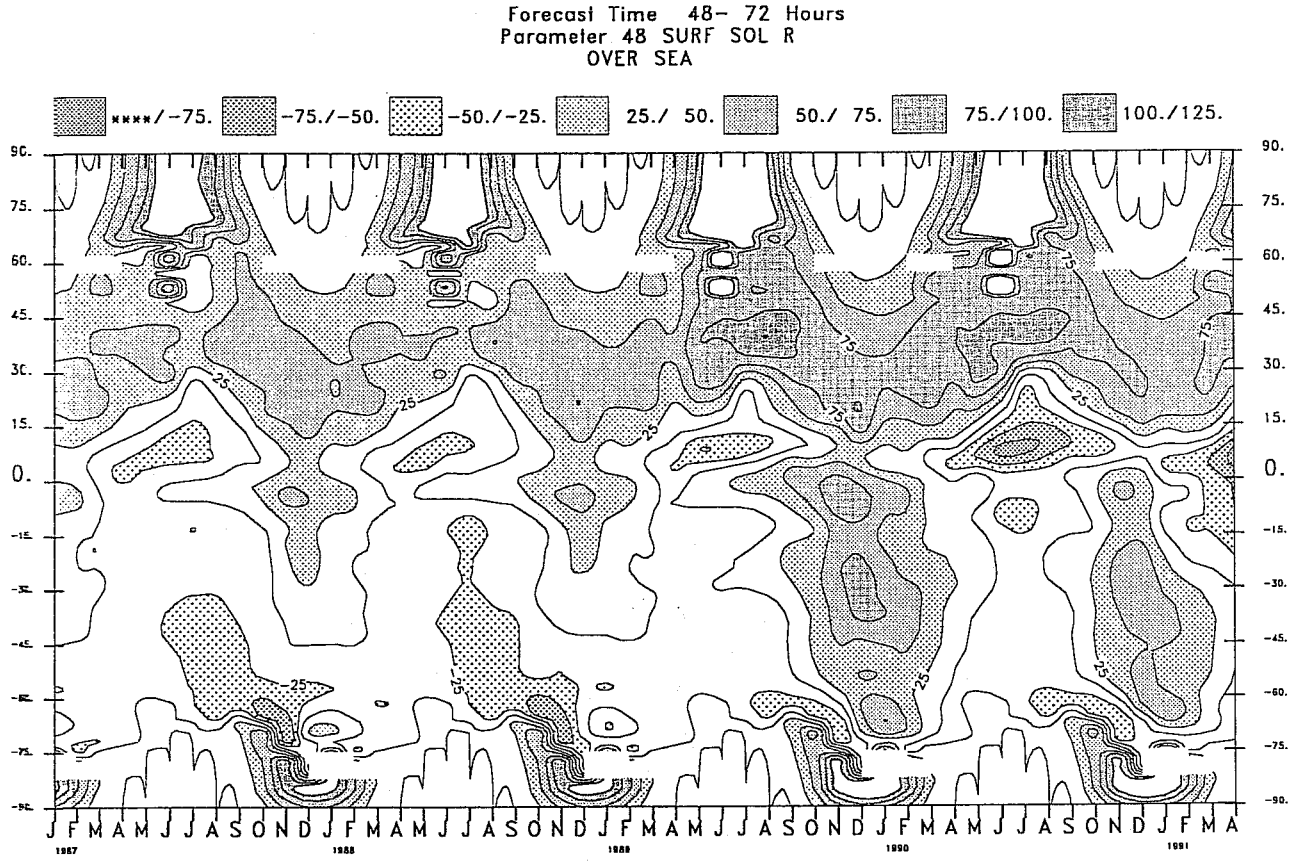

Fig. 5 Time evolution of the zonally averaged difference with Oberhuber's (1989) climatology of the net shortwave radiation at the ocean surface. Units are W m^{-2}.

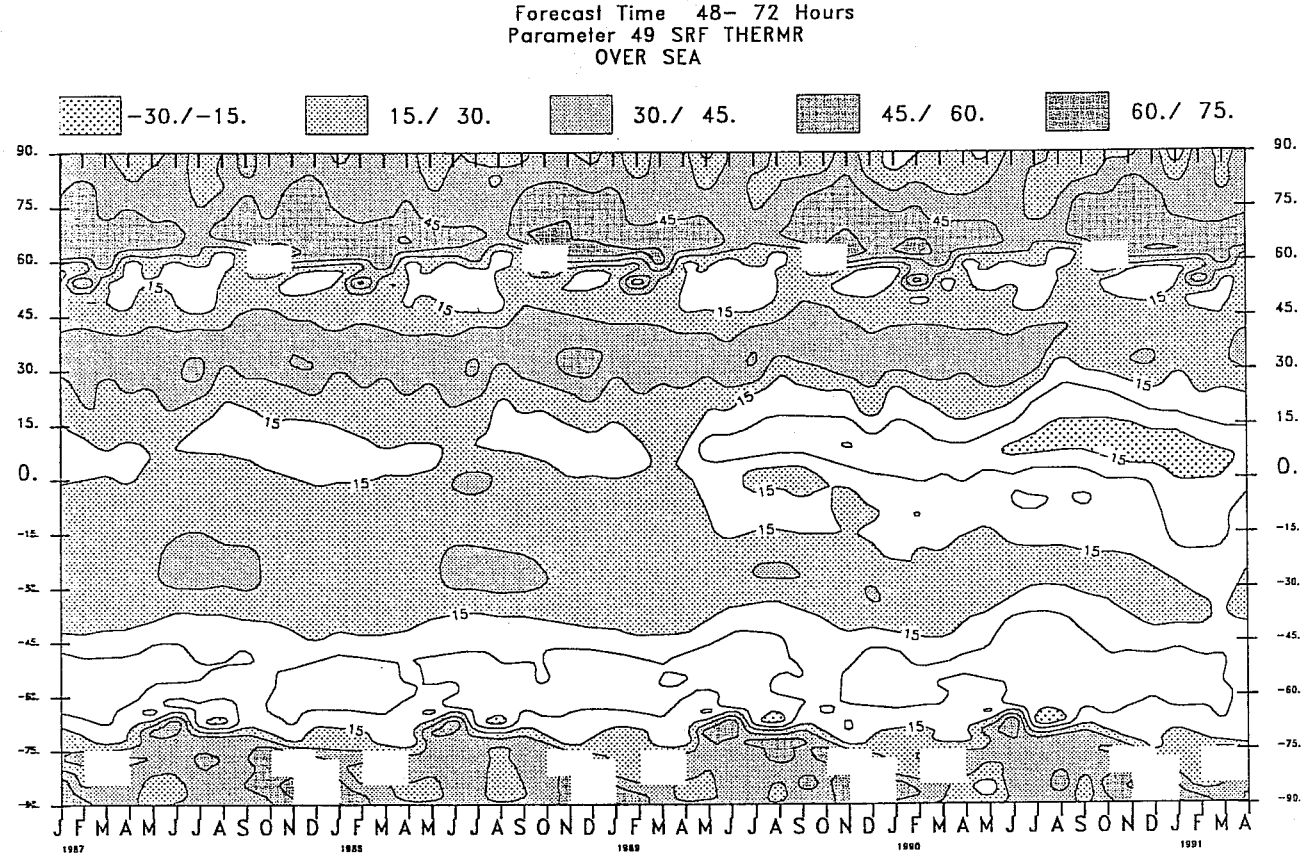

Fig. 6 As in Fig.5, but for net longwave radiation at the ocean surface.

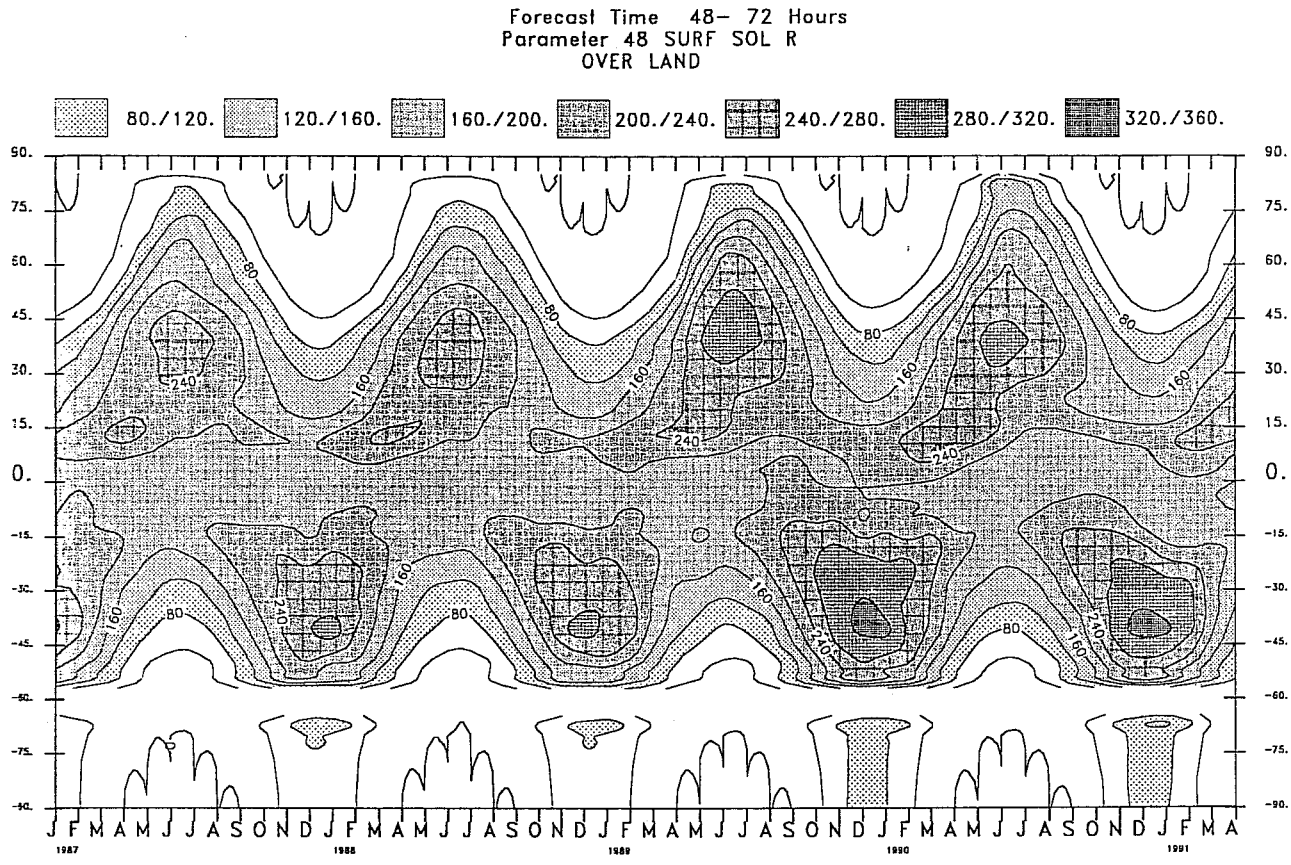

Fig. 7 Time evolution of the zonally averaged net shortwave radiation over land. Units are W m^{-2}.

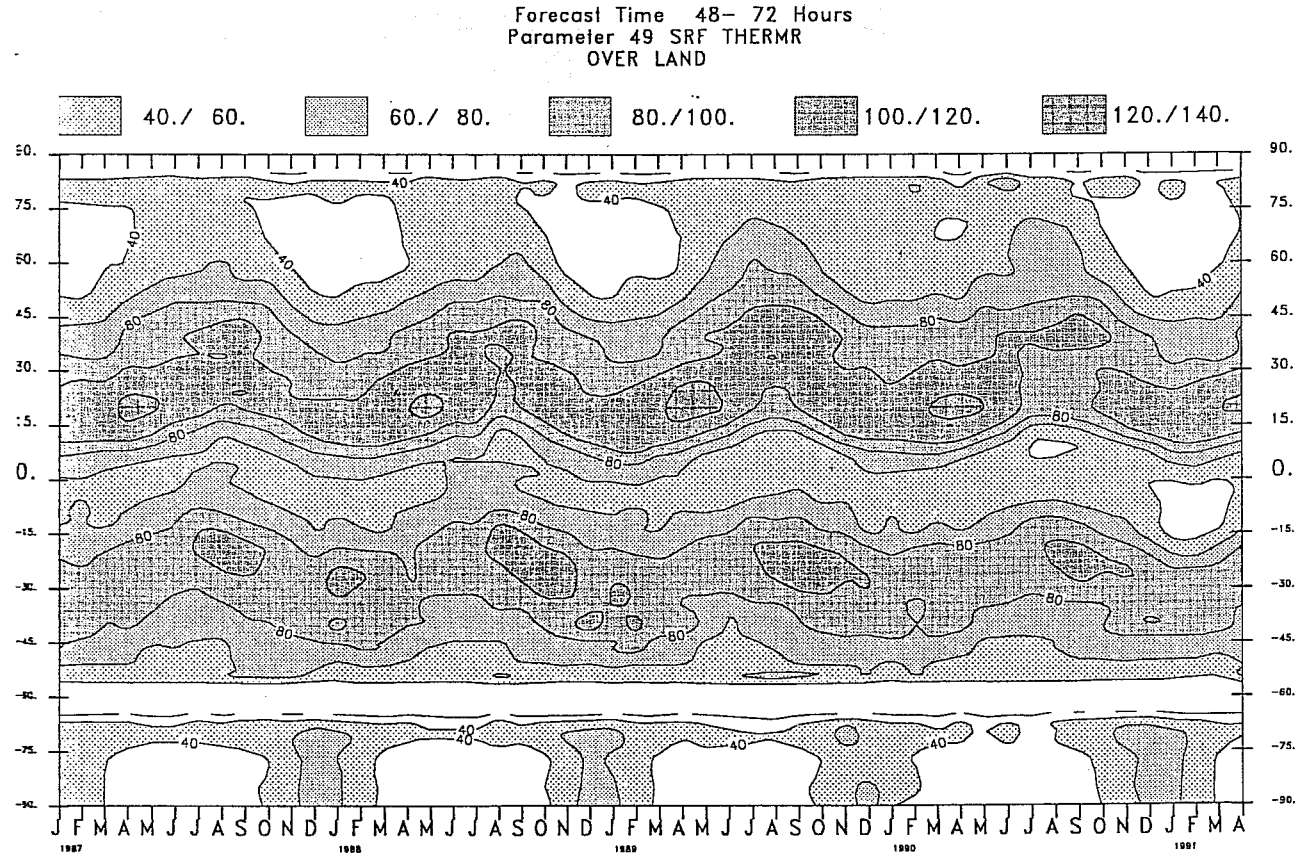

Fig. 8 As in Fig.7, but for net longwave radiation.

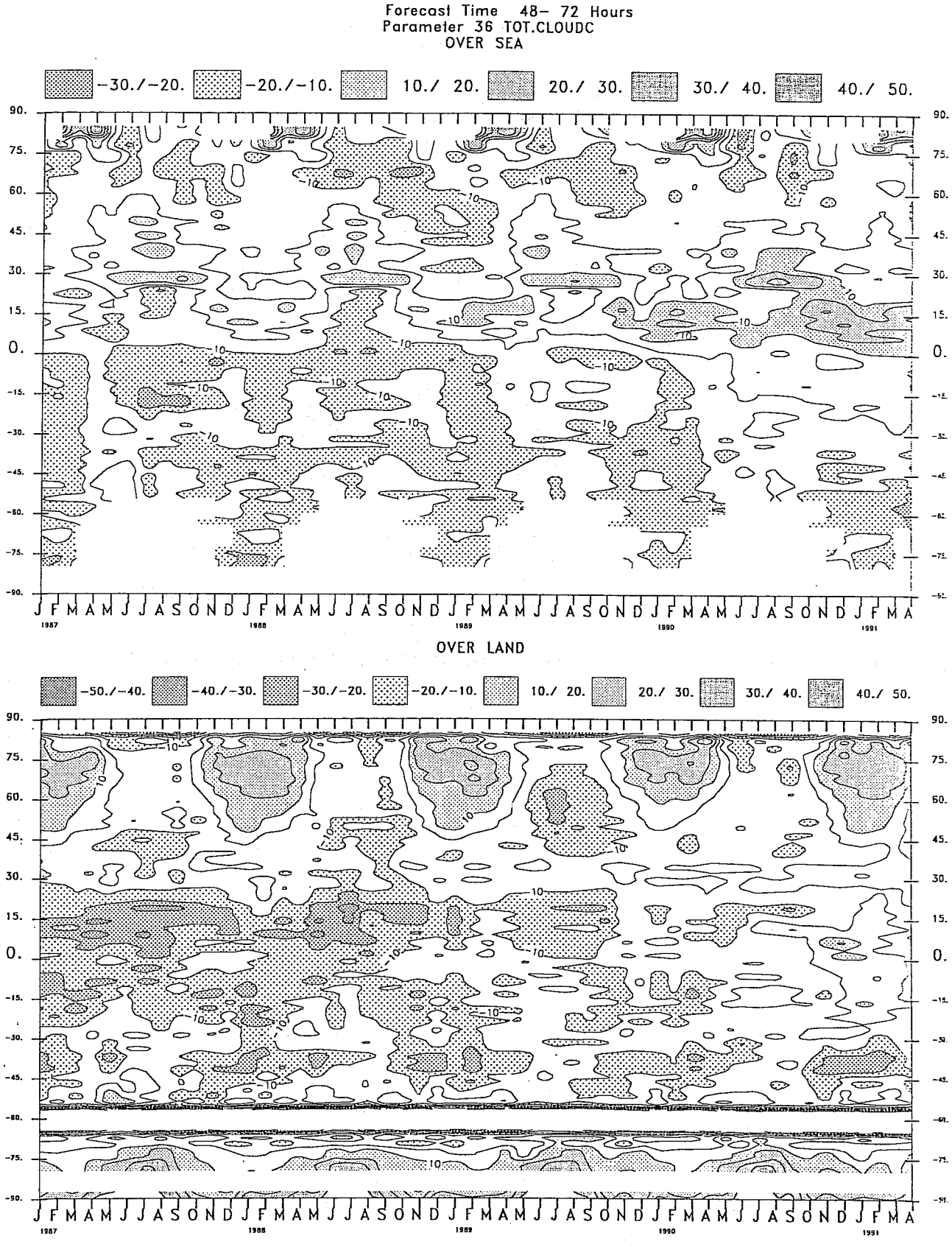

Fig. 9 Time evolution of the zonally averaged difference with the Surface Cloud Climatology of the total cloud cover over the ocean (top) and over land (bottom). Units are percent.

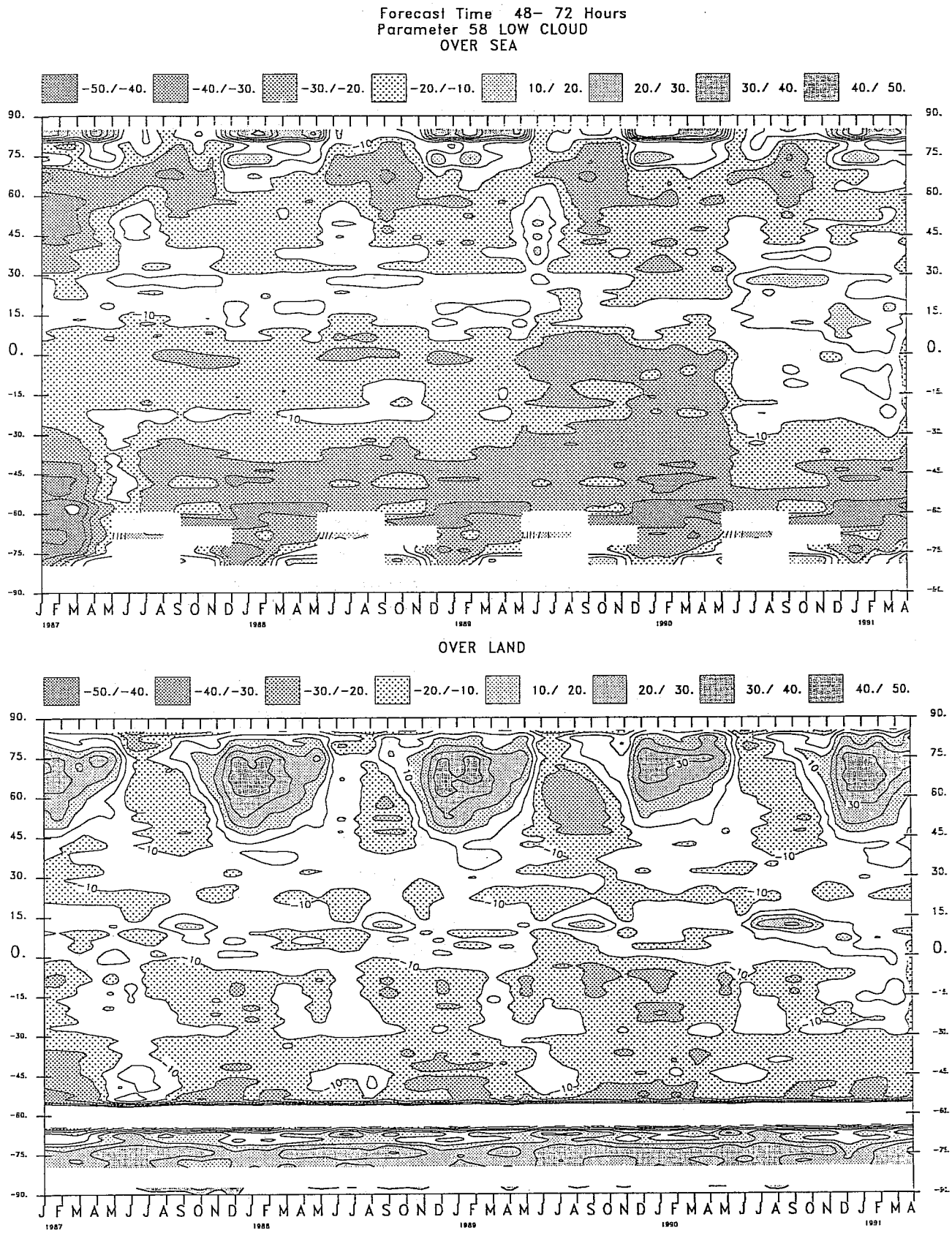

Fig. 10 Time evolution of the zonally averaged difference with the Surface Cloud Climatology of the low-level cloudiness over the ocean (top) and over land (bottom). Units are percent.

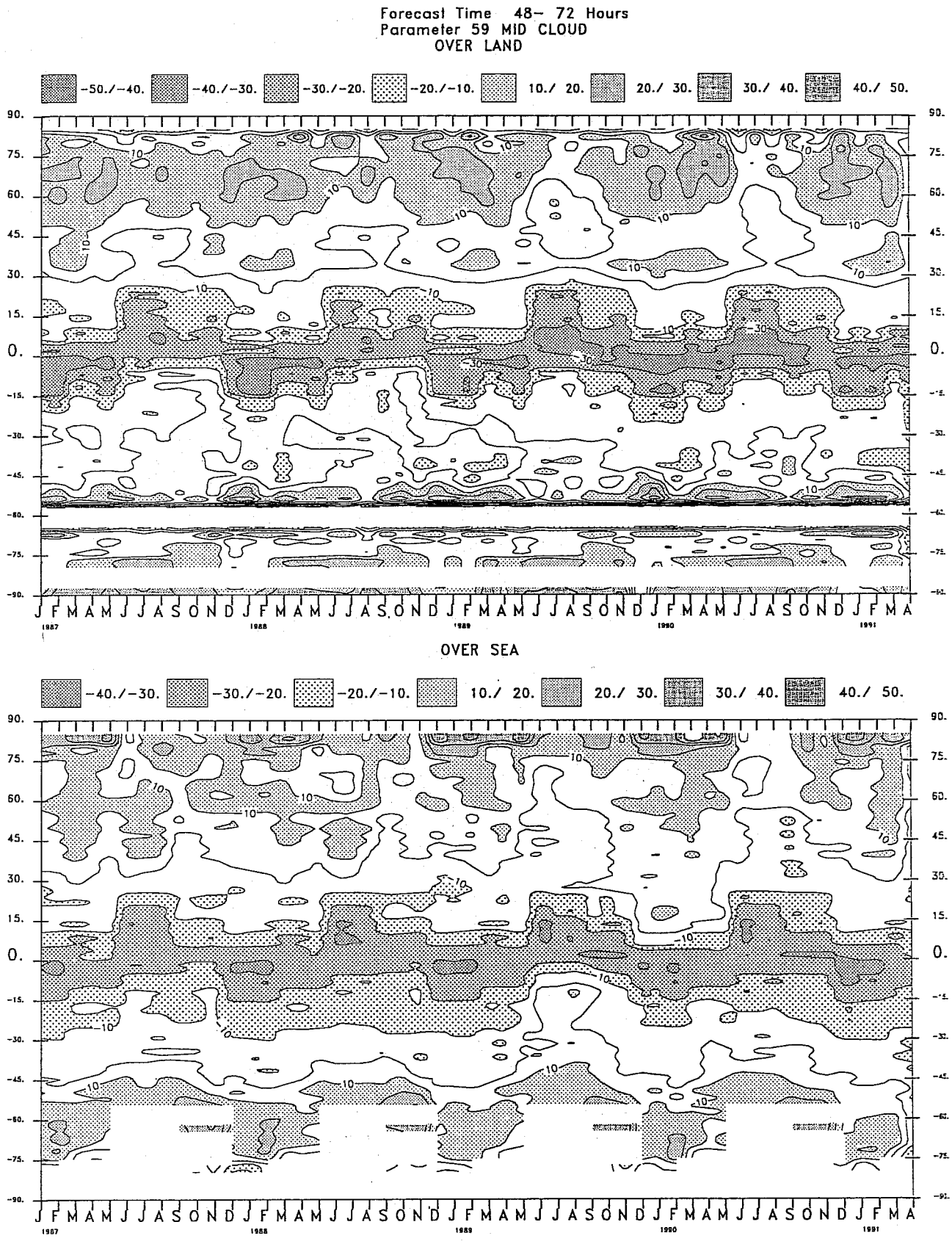

Fig. 11 Time evolution of the zonally averaged difference with the Surface Cloud Climatology of the middle-level cloudiness over the ocean (top) and over land (bottom). Units are percent.

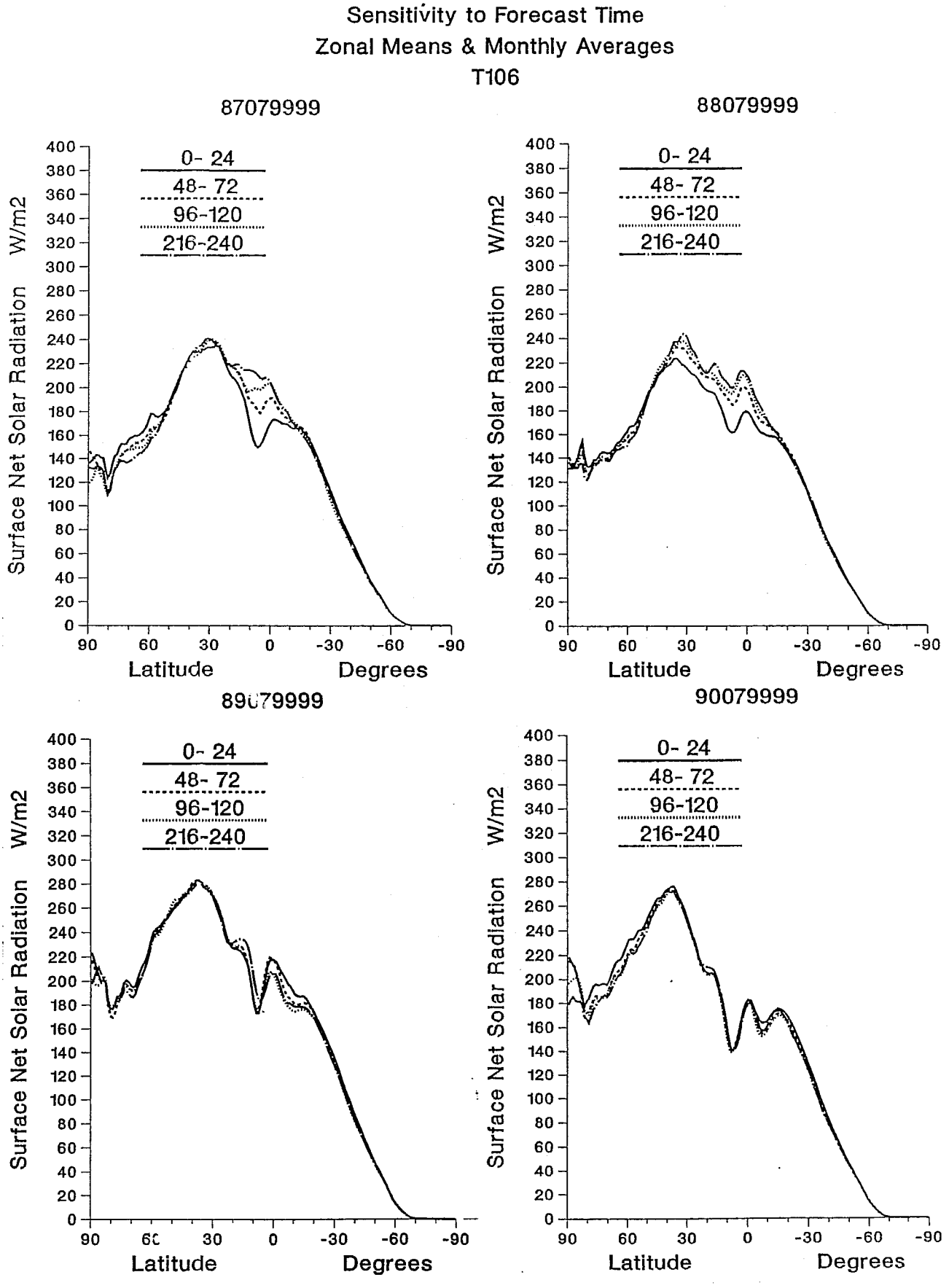

Fig. 12 The zonal means of the surface net solar radiation averaged over day 1, 3, 5 and 9 for the 4 months of July 1987-1990. Units are W m^{-2}.

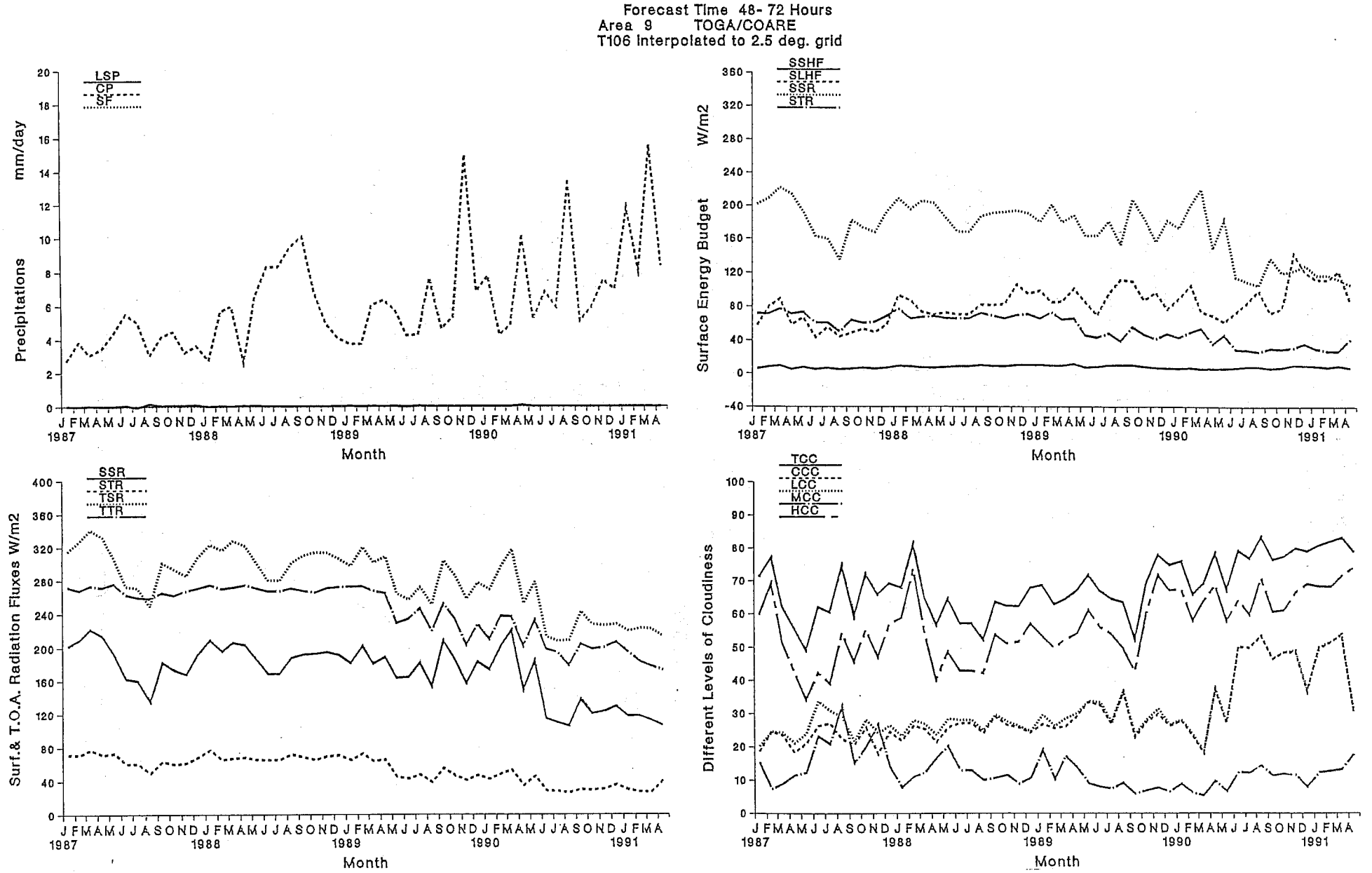

Fig. 13 The time evolution of the precipitation, surface and TOA radiation budgets and cloudiness over the TOGA/COARE area.

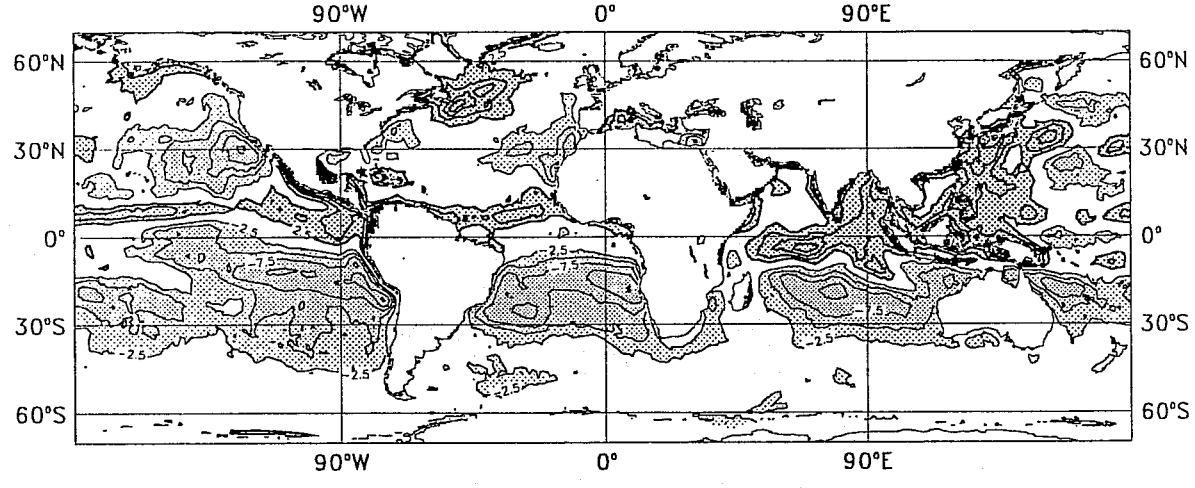

Fig. 14a Difference between the mean SSM/I derived PWC and the mean ECMWF analysis PWC for July 1990. Units: kg/m^2. Contours ±2.5, ±5.0, ...

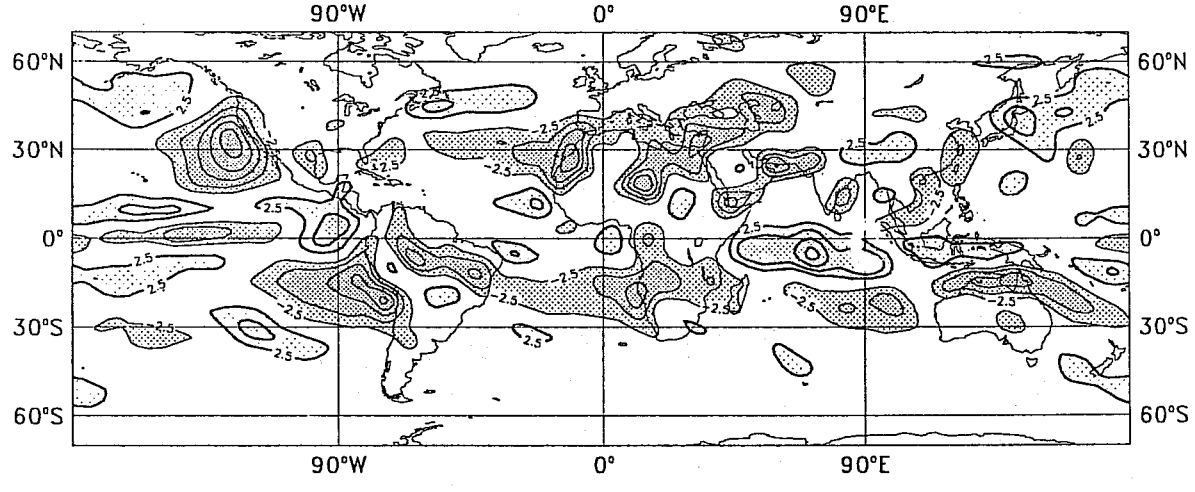

Fig. 14b Difference between the mean PWC of the 5-day forecast and the analysis for July 1990. Units: kg/m^2. Contours ±2.5, ±5.0, ...

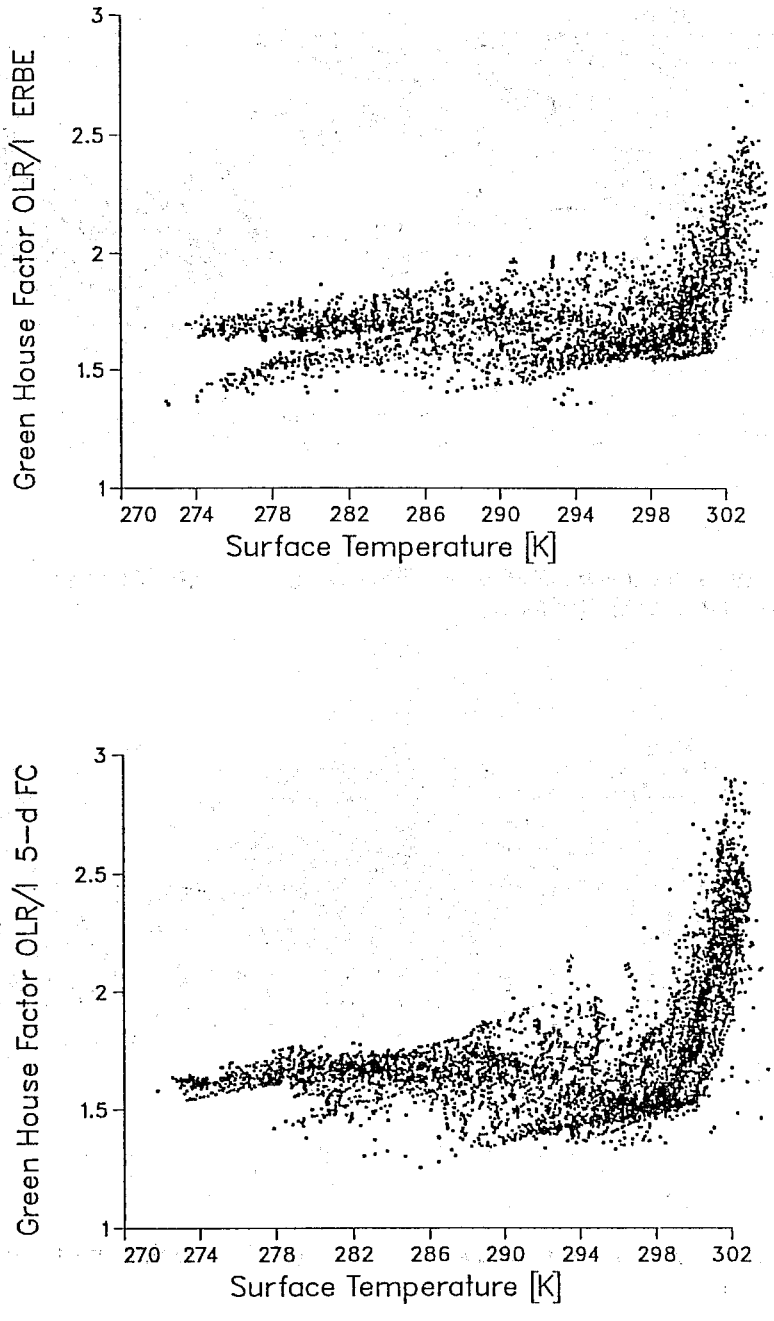

Fig. 15 Scatter diagram for the greenhouse factor versus the surface temperature. Upper panel uses ERBE data of July 1985 for the OLR. Lower panel uses the 6-hour forecast radiation fluxes of July 1990 for the OLR.

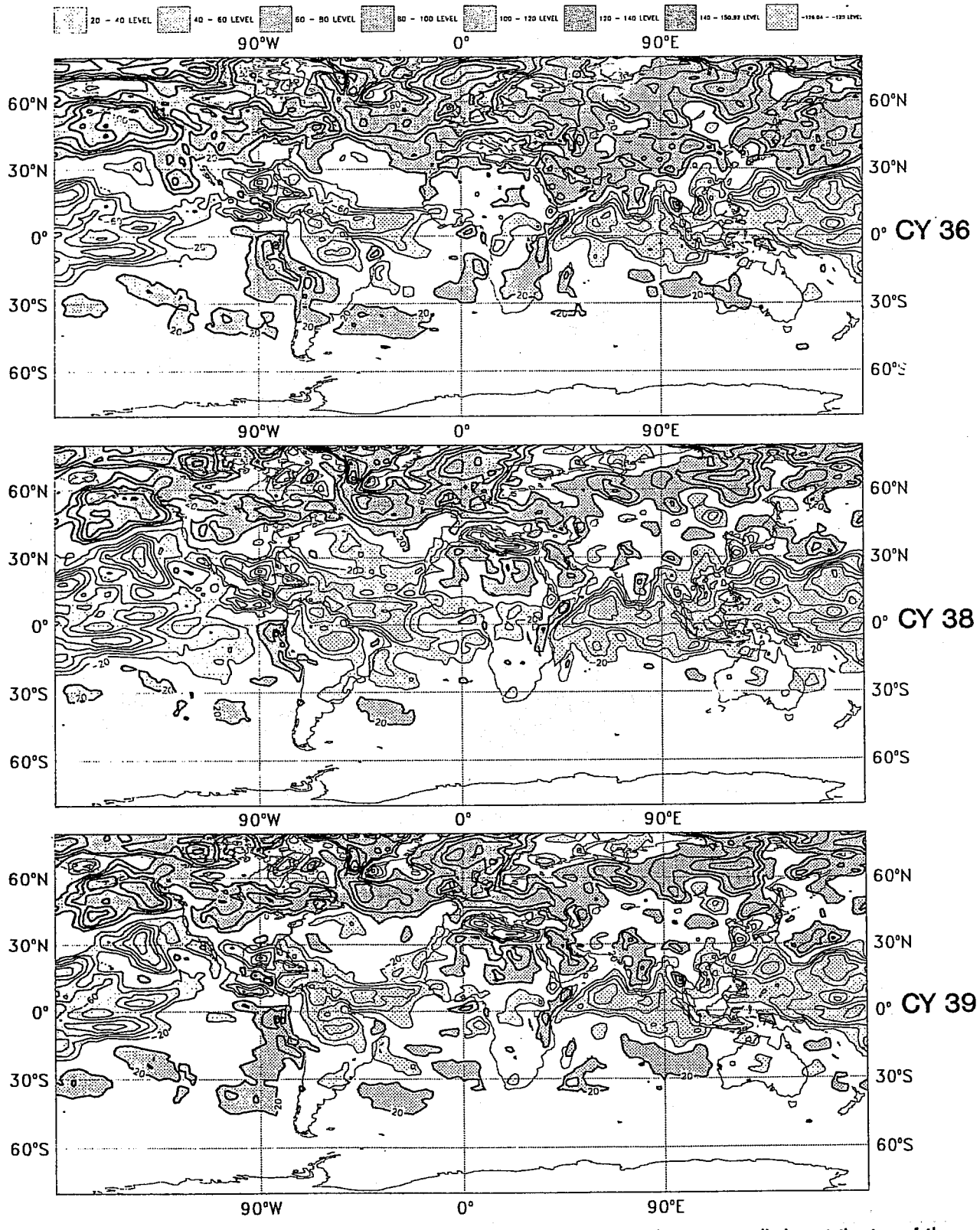

Fig. 16 The difference with ERBE observations (July 1985) of the net shortwave radiation at the top of the atmosphere for July 1990. Units are W m^{-2}. Top panel is for the cycle 36 version of the ECMWF model, middle panel for cycle 38 and bottom panel for cycle 39.

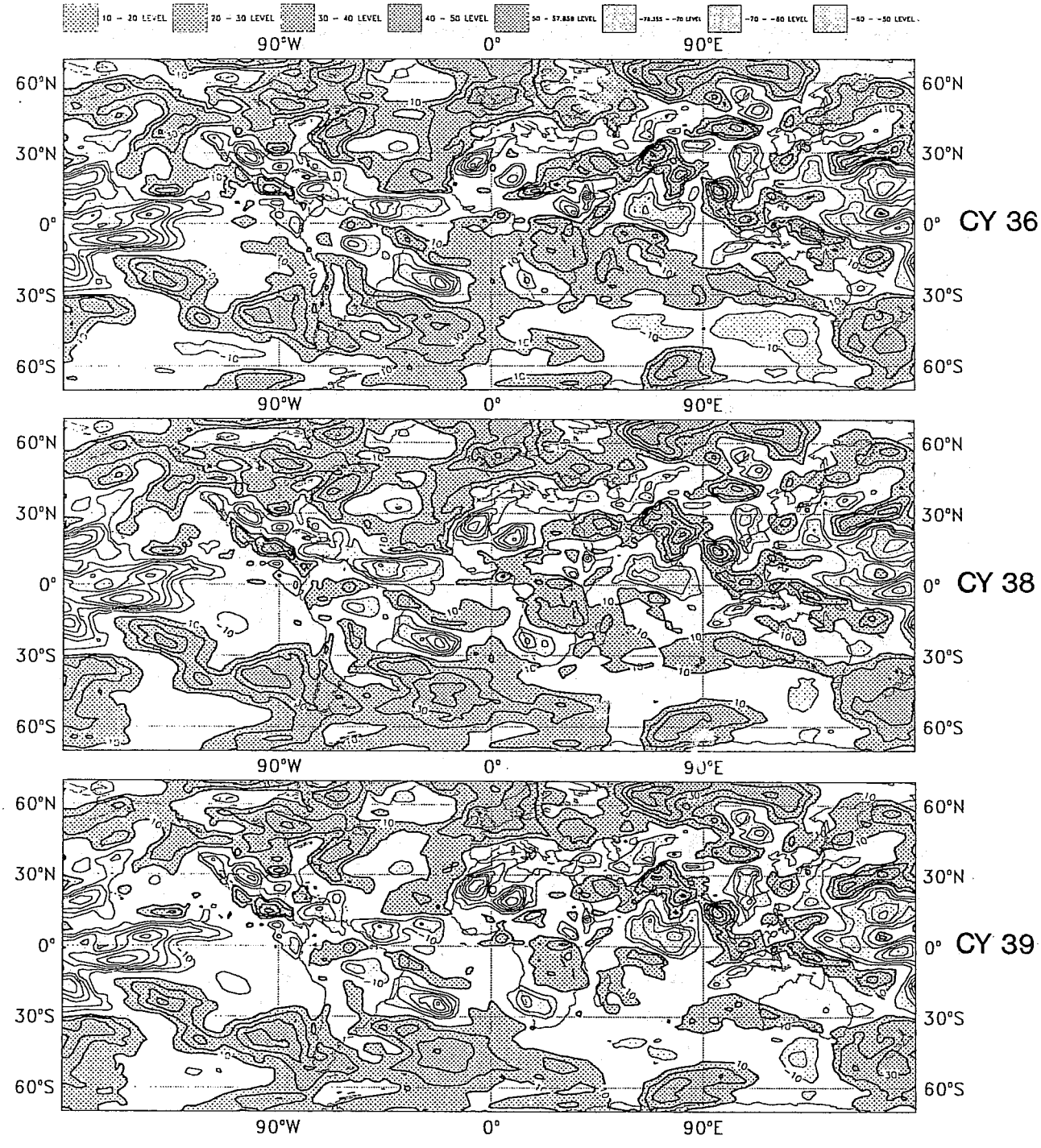

Fig. 17 As in Fig. 16, but for the outgoing longwave radiation.

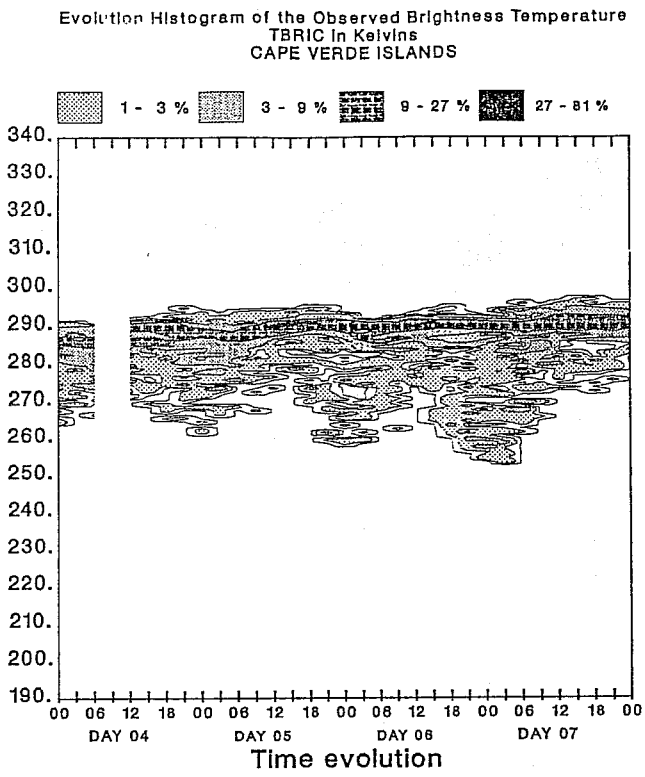

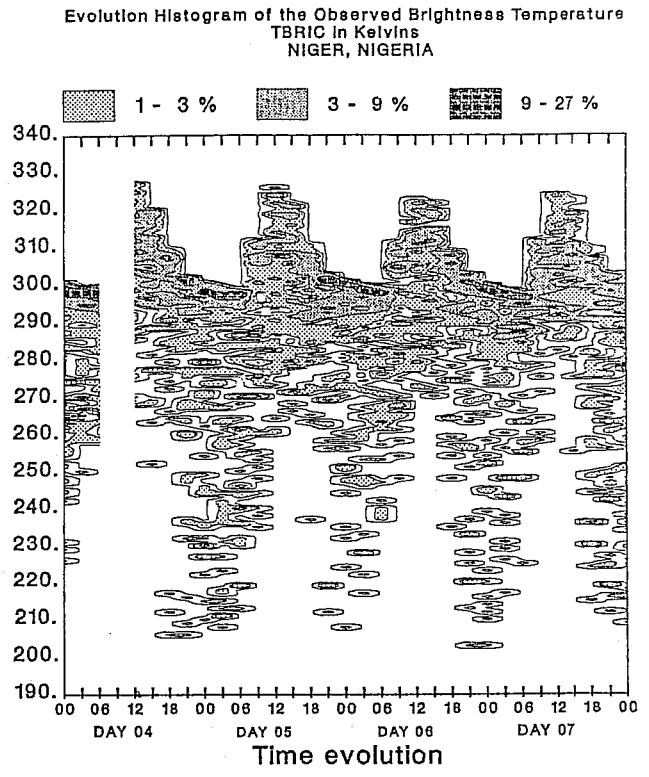

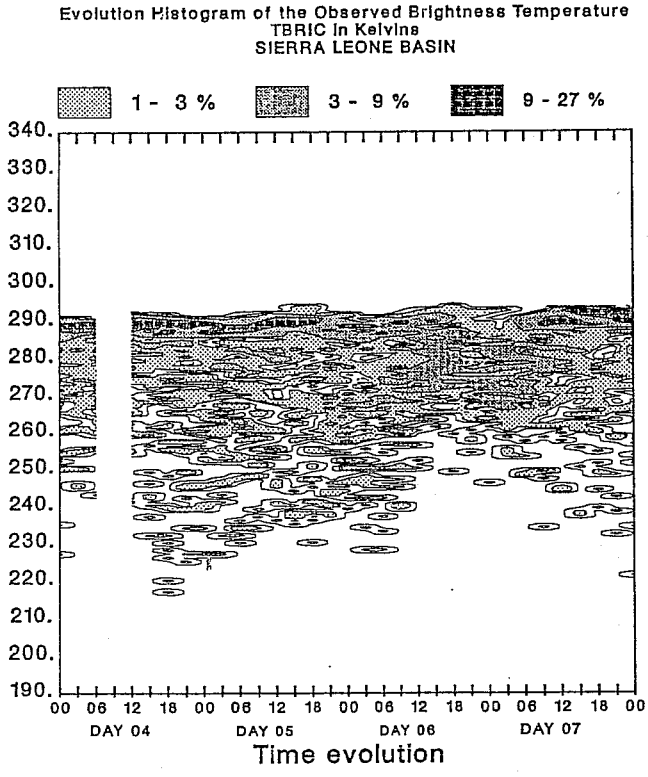

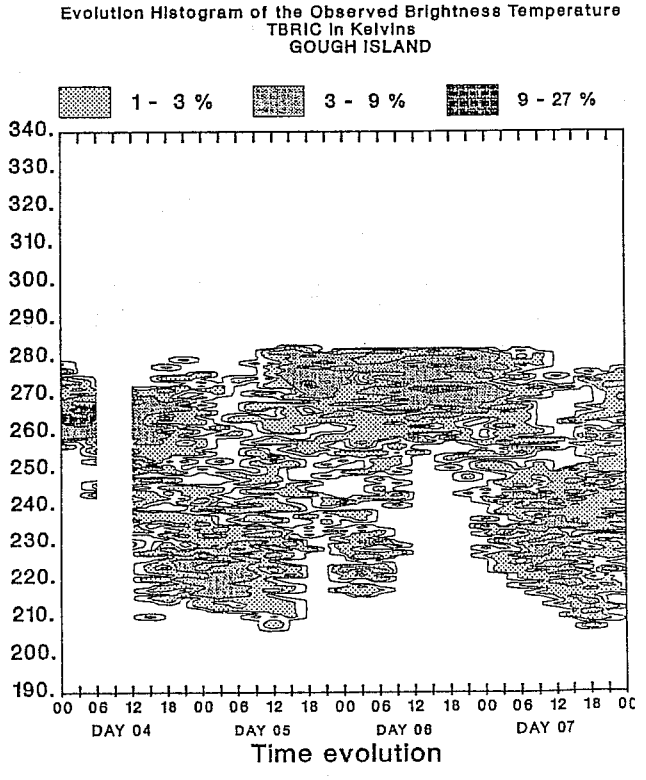

Fig. 18 The evolution histogram of the longwave window brightness temperature observed by Meteosat between 4 July 1983, 00Z and 8 July 1983, 00Z. Results are shown over four limited areas:

Cape Verde Island	26N-16N	28W-18W	stratiform clouds
Niger, Nigeria	20N-10N	5W- 5E	convection over land
Sierra Leone Basin	16N- 6N	34W-24W	convection over ocean
Gough Island	39S-49S	16W- 6W	S.H. frontal systems

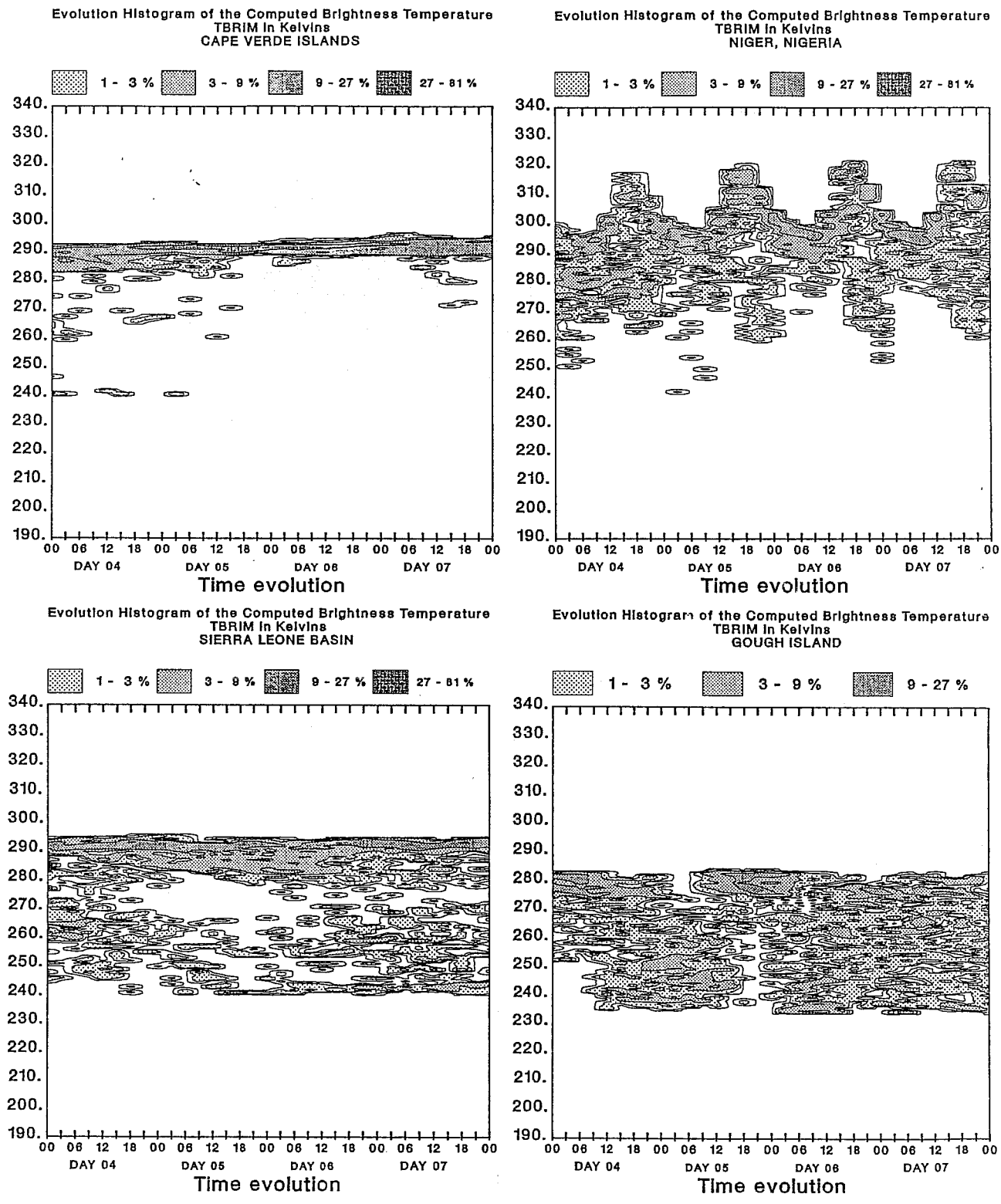

Fig. 19 As in Fig. 18, but for the brightness temperature simulated with the CY31 version of the ECMWF model.

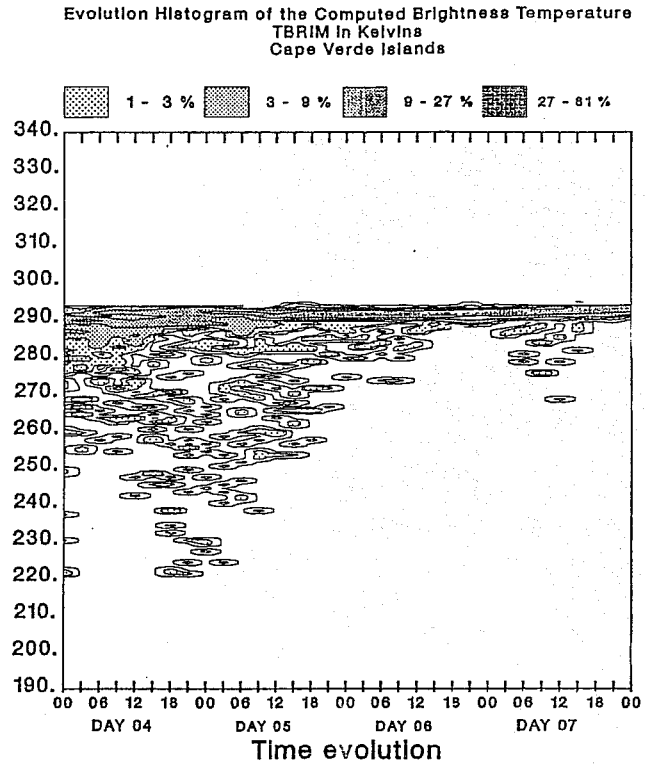

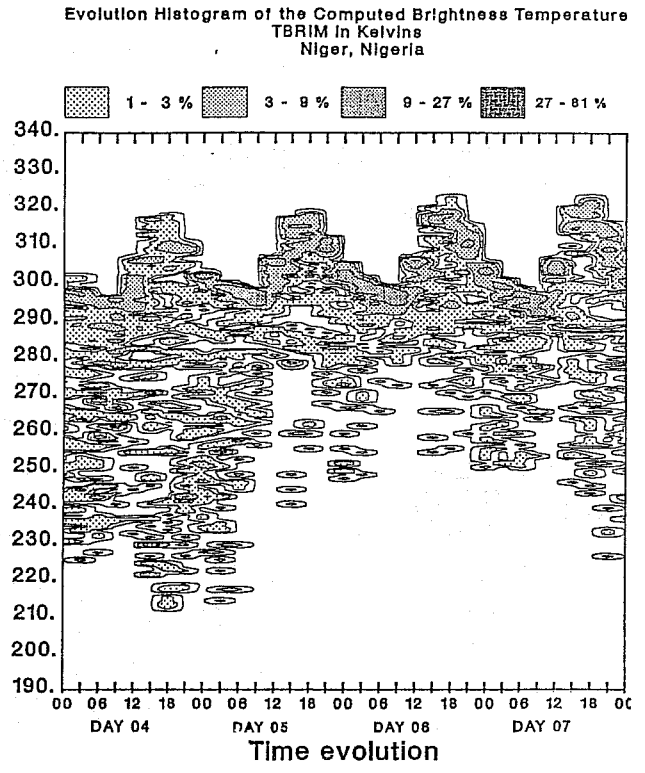

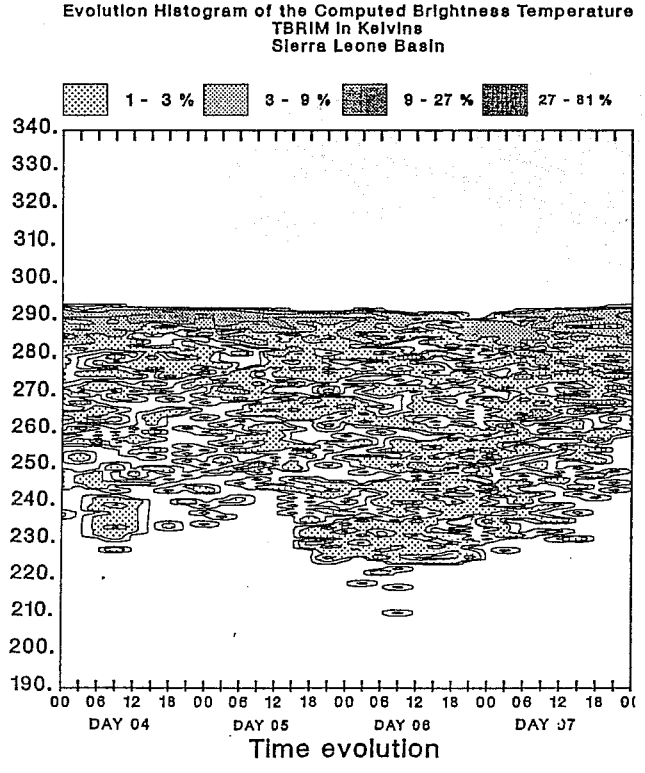

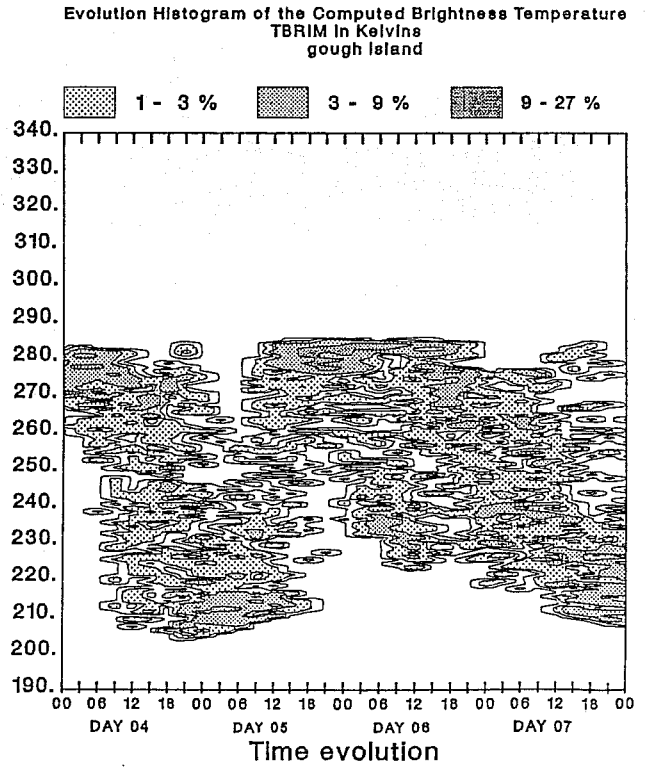

Fig. 20 As in Fig. 18, but for the brightness temperature simulated with the CY36 version of the ECMWF model.

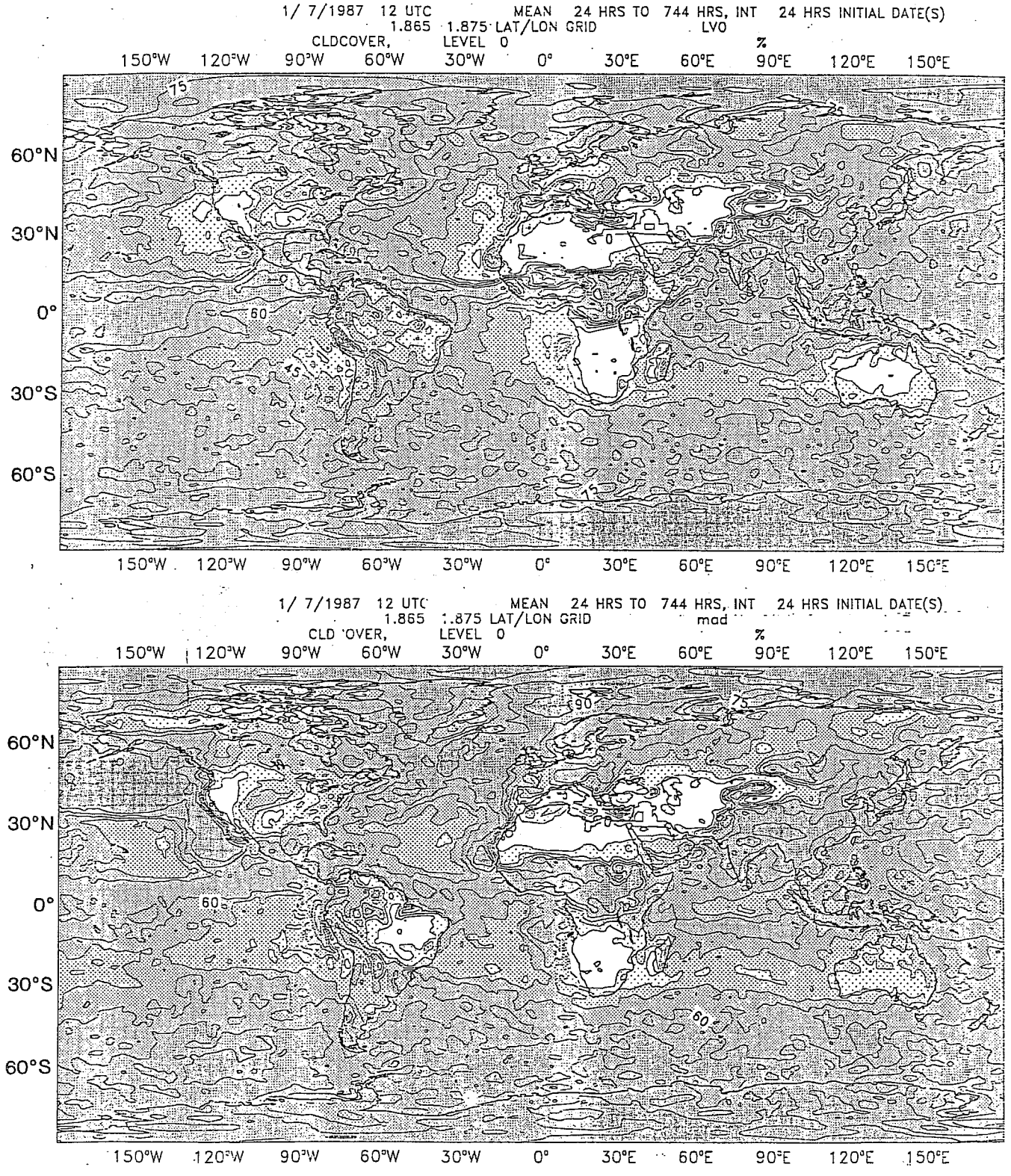

Fig. 21 The geographical distribution of the total cloudiness as given in CY36 model (top panel) and SC (bottom panel) experiments.

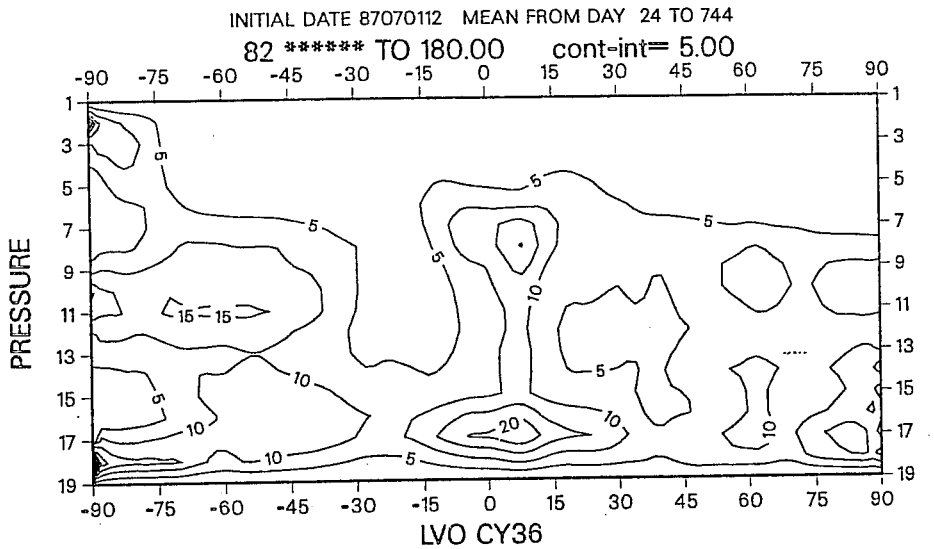

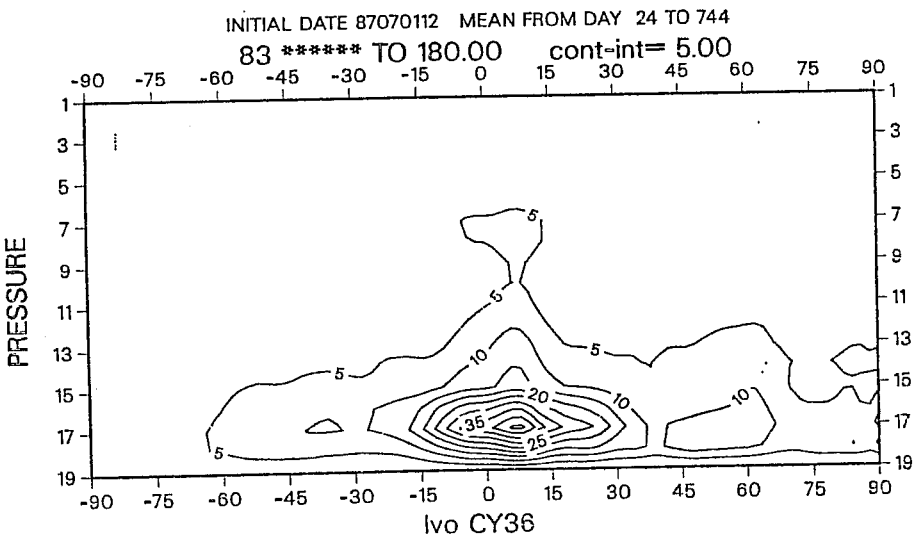

Fig. 22 **The height-latitude cross-section of the zonally averaged cloudiness (top panel) and cloud liquid water path (bottom panel)in a T63 simulation of July 1987 with the operational CY36 model.**

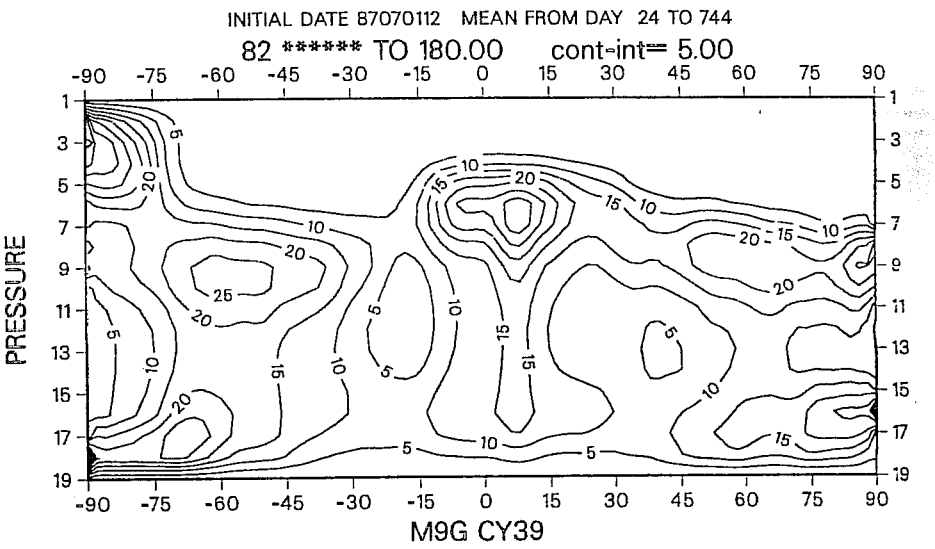

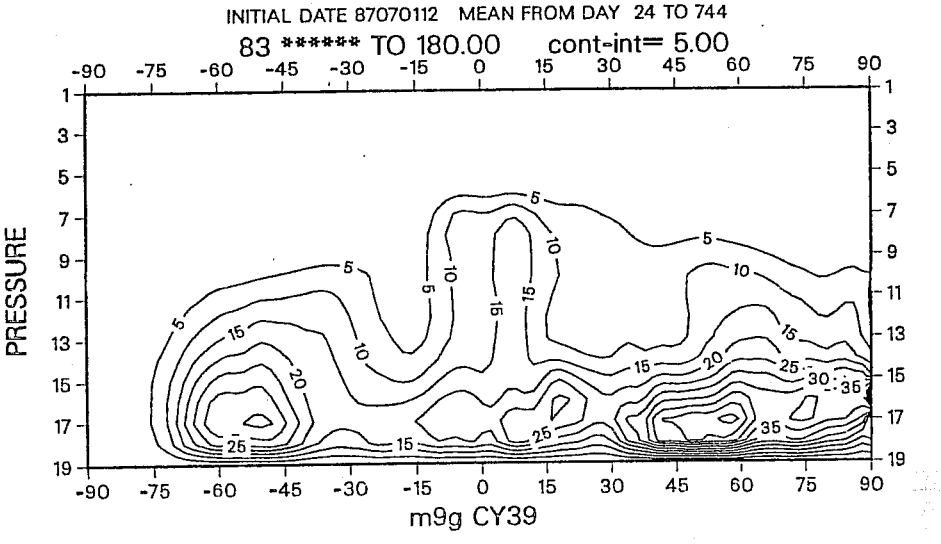

Fig. 23 **As in Fig. 22, but with the operational CY39 model.**

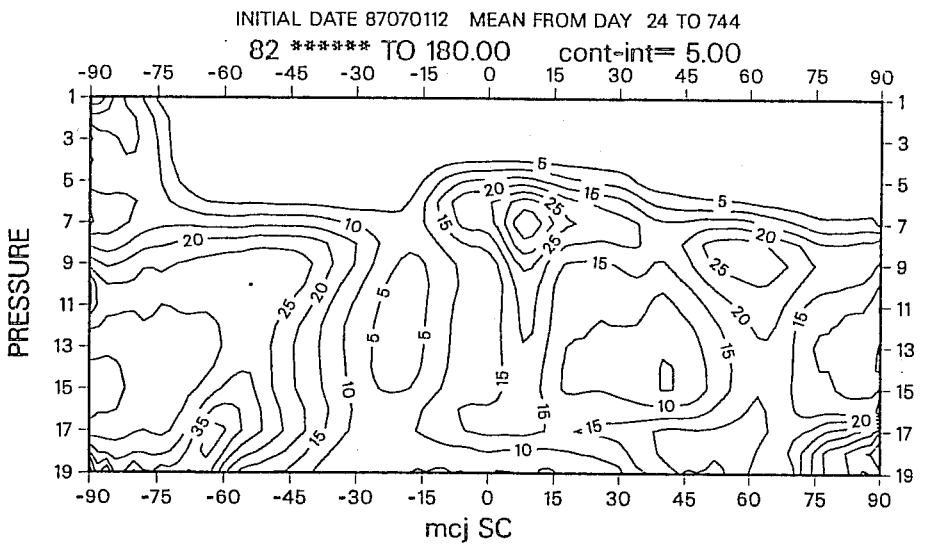

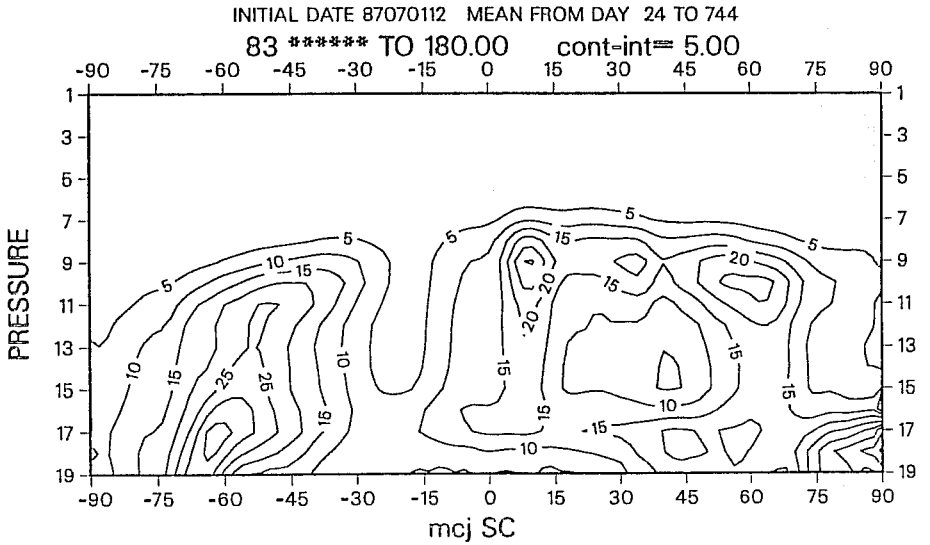

Fig. 24 As in Fig. 22, but for a model with the SC configuration.

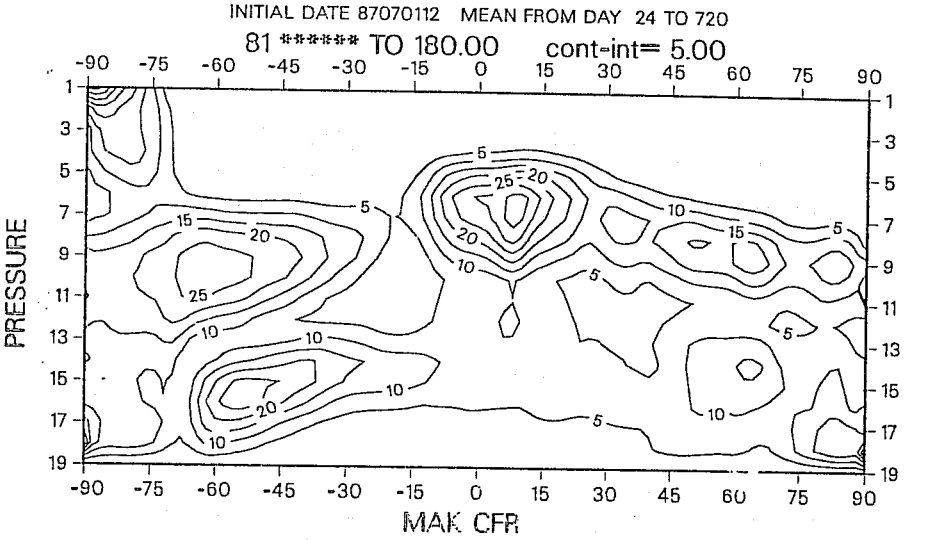

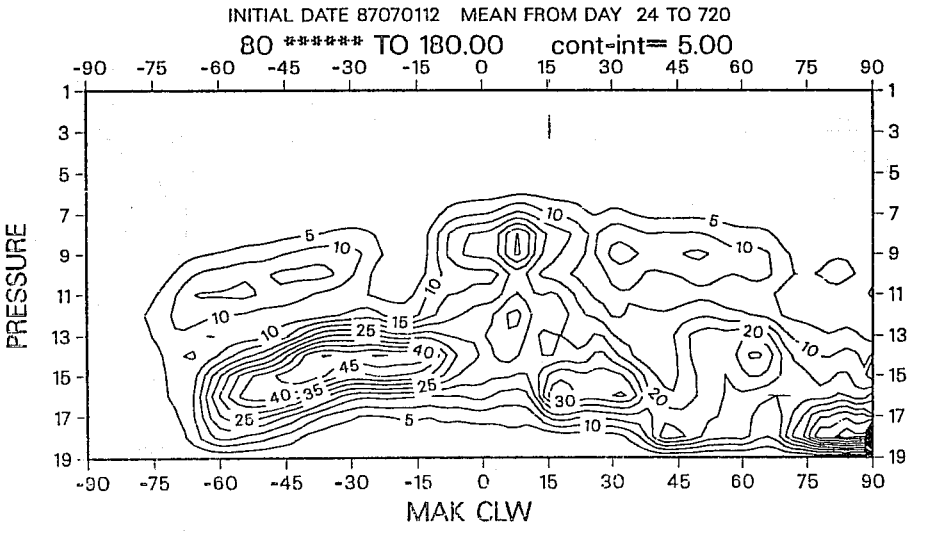

Fig. 25 As in Fig. 22, but for a model with the UN configuration.

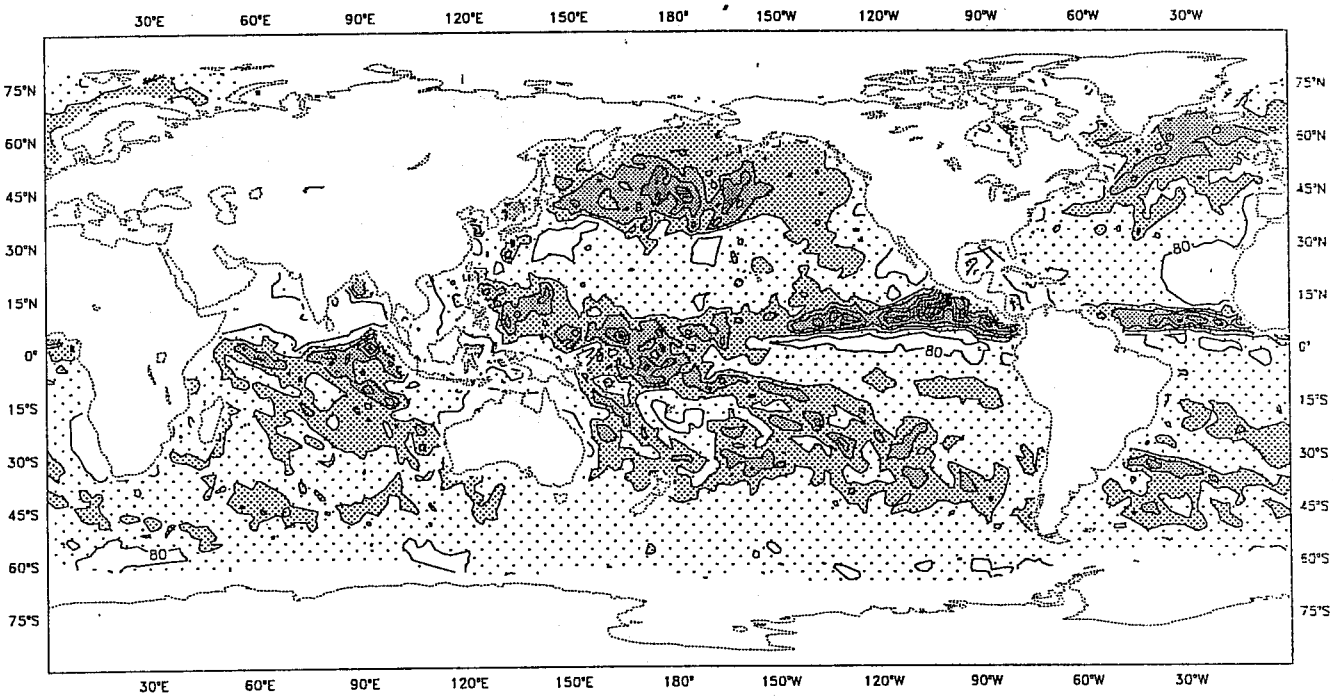

Fig. 26 The geographical distribution of the vertically integrated cloud liquid water over the ocean as deduced from SSM/I observations and computed by the 4 model simulations.

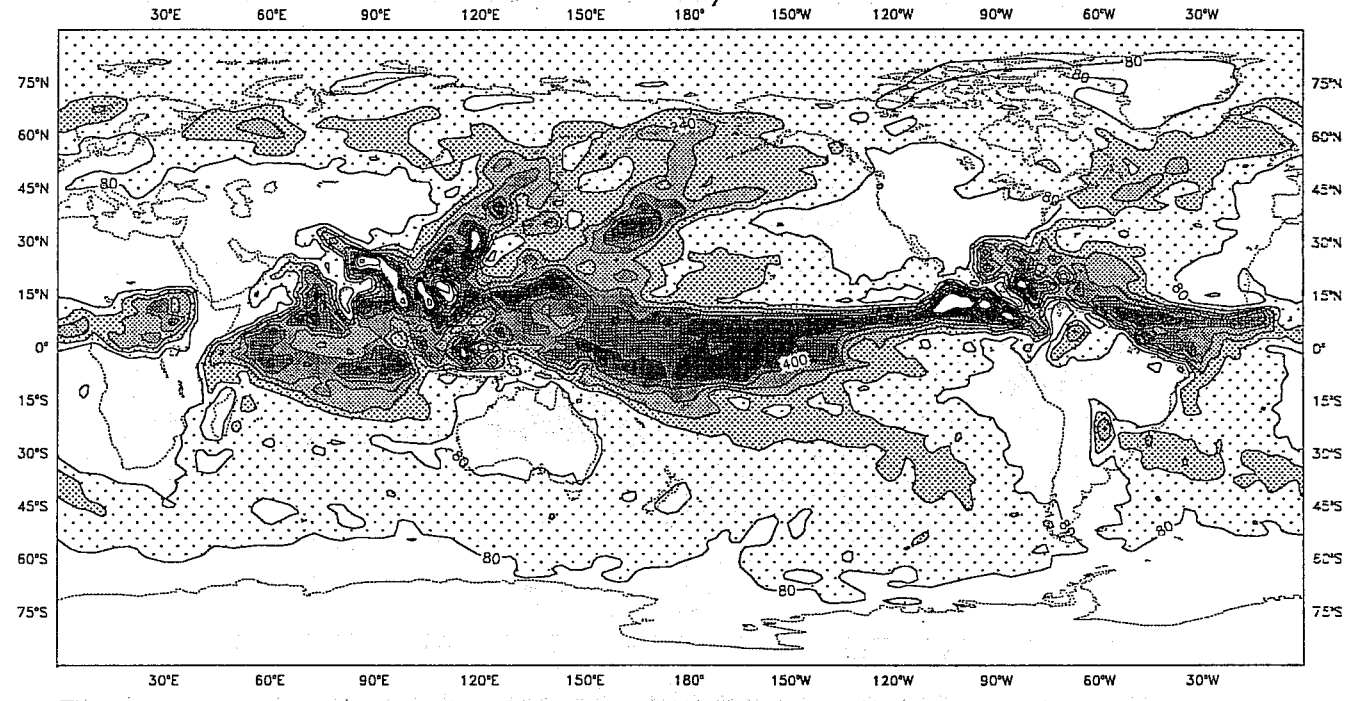

Fig. 26 b)

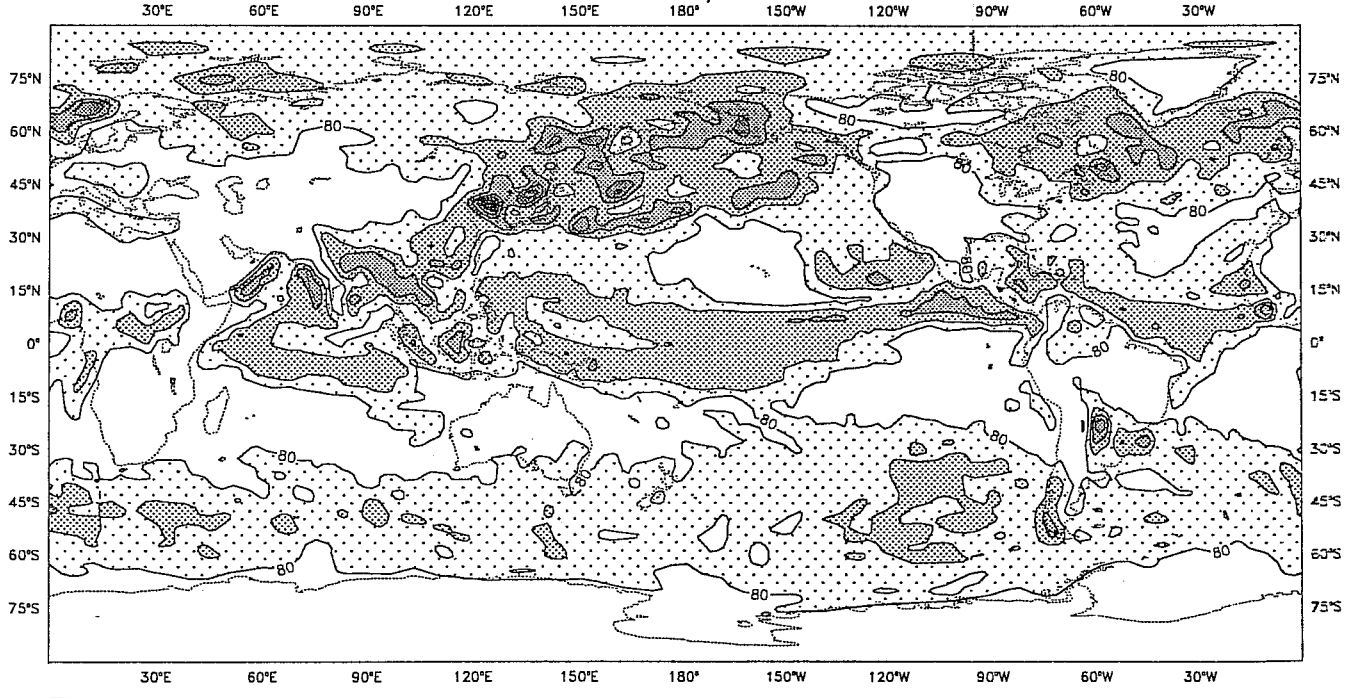

Fig. 26 c)

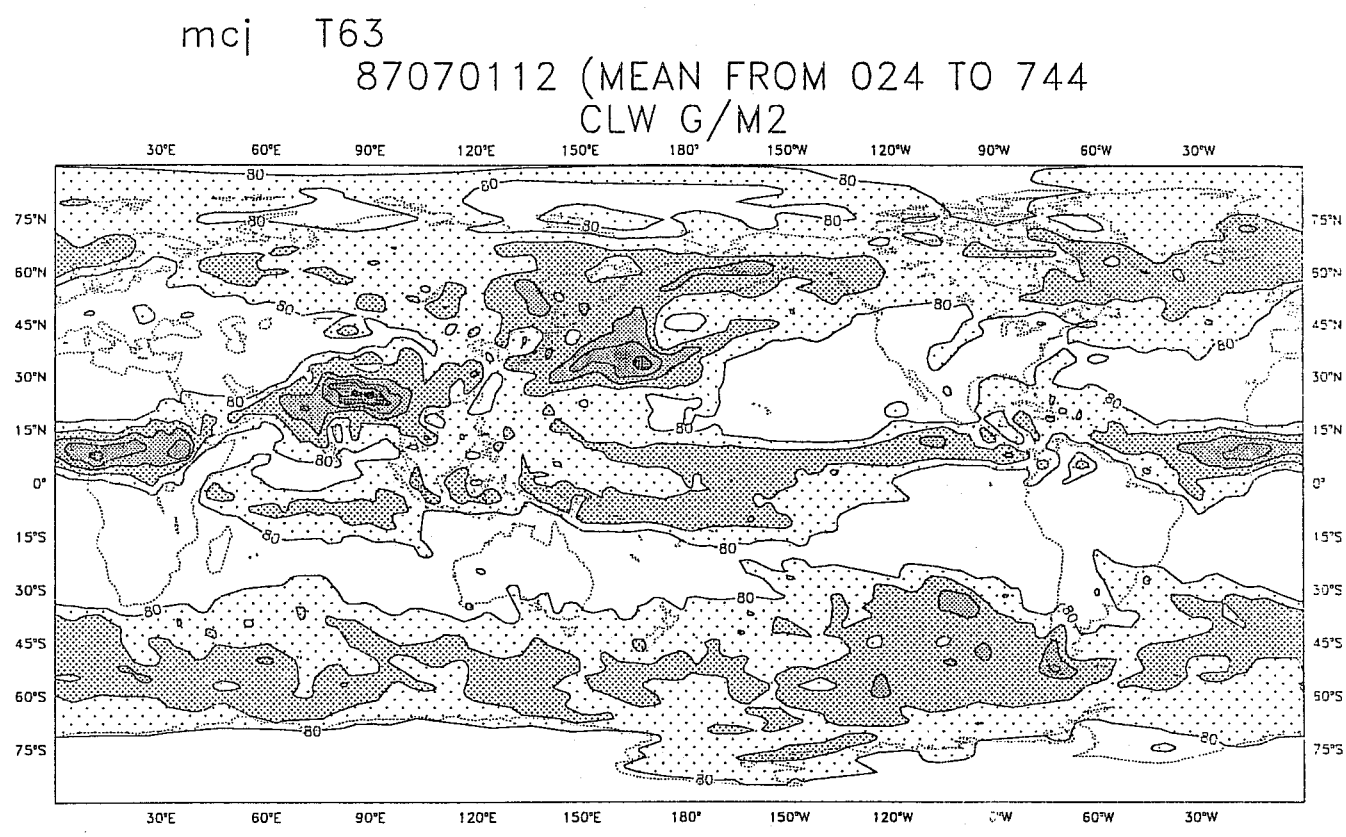

Fig. 26 d)

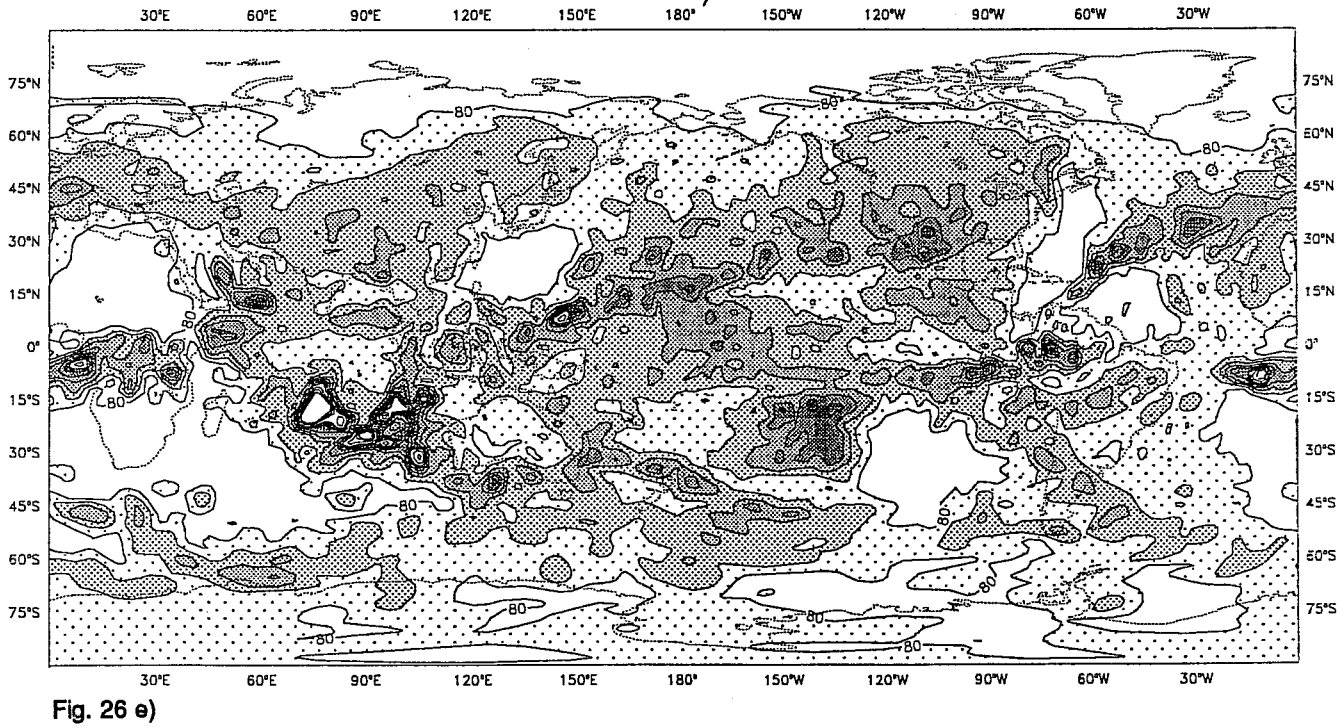

Fig. 26 e)

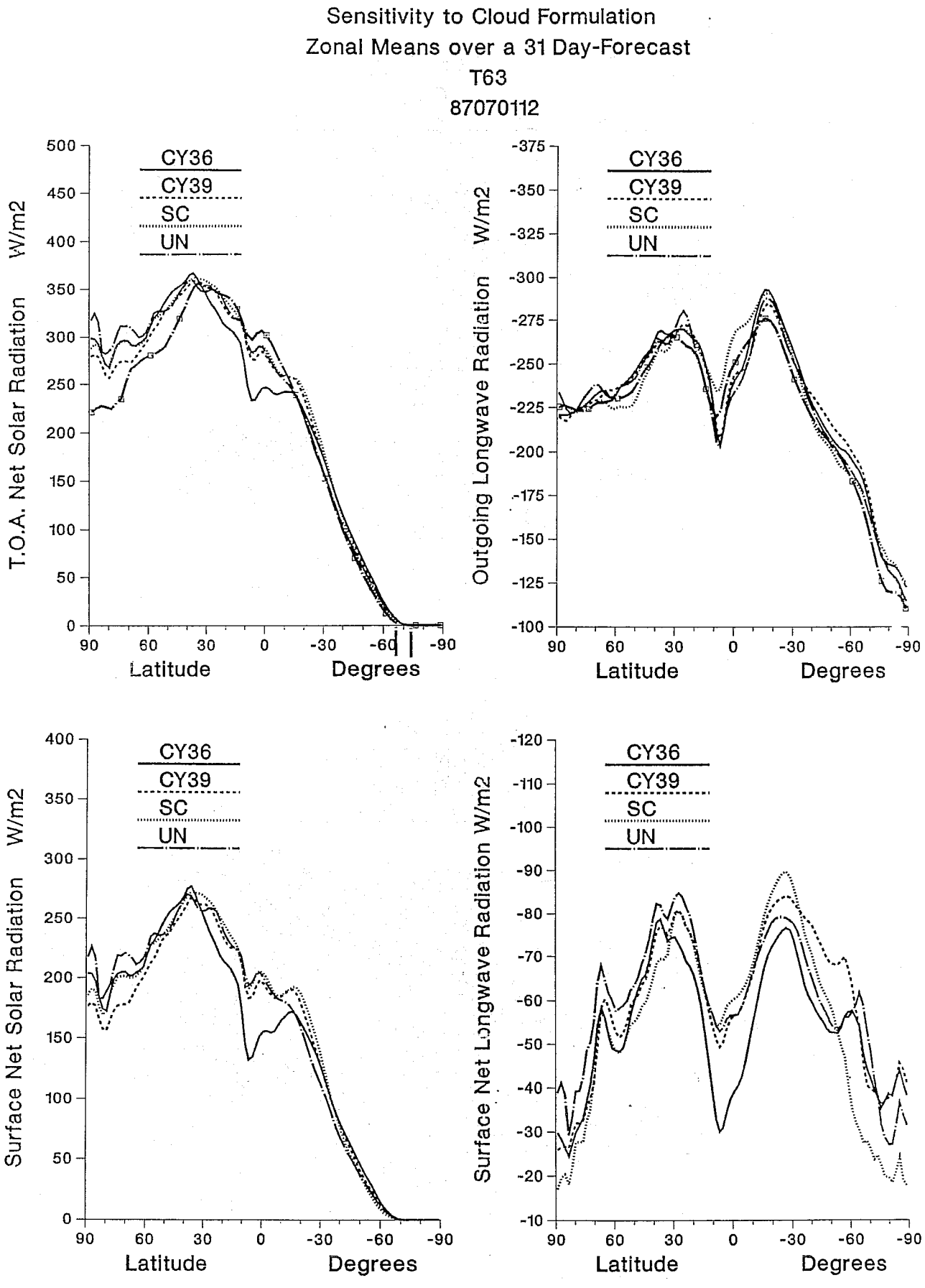

Fig. 27 The zonally averaged shortwave (left panels) and longwave (right panels) radiative fluxes at TOA (top panels) and at the surface (bottom panels) from the 4 model experiments. Units are W m^{-2}. TOA ERBE fluxes are given by the dot-dash line with squares.

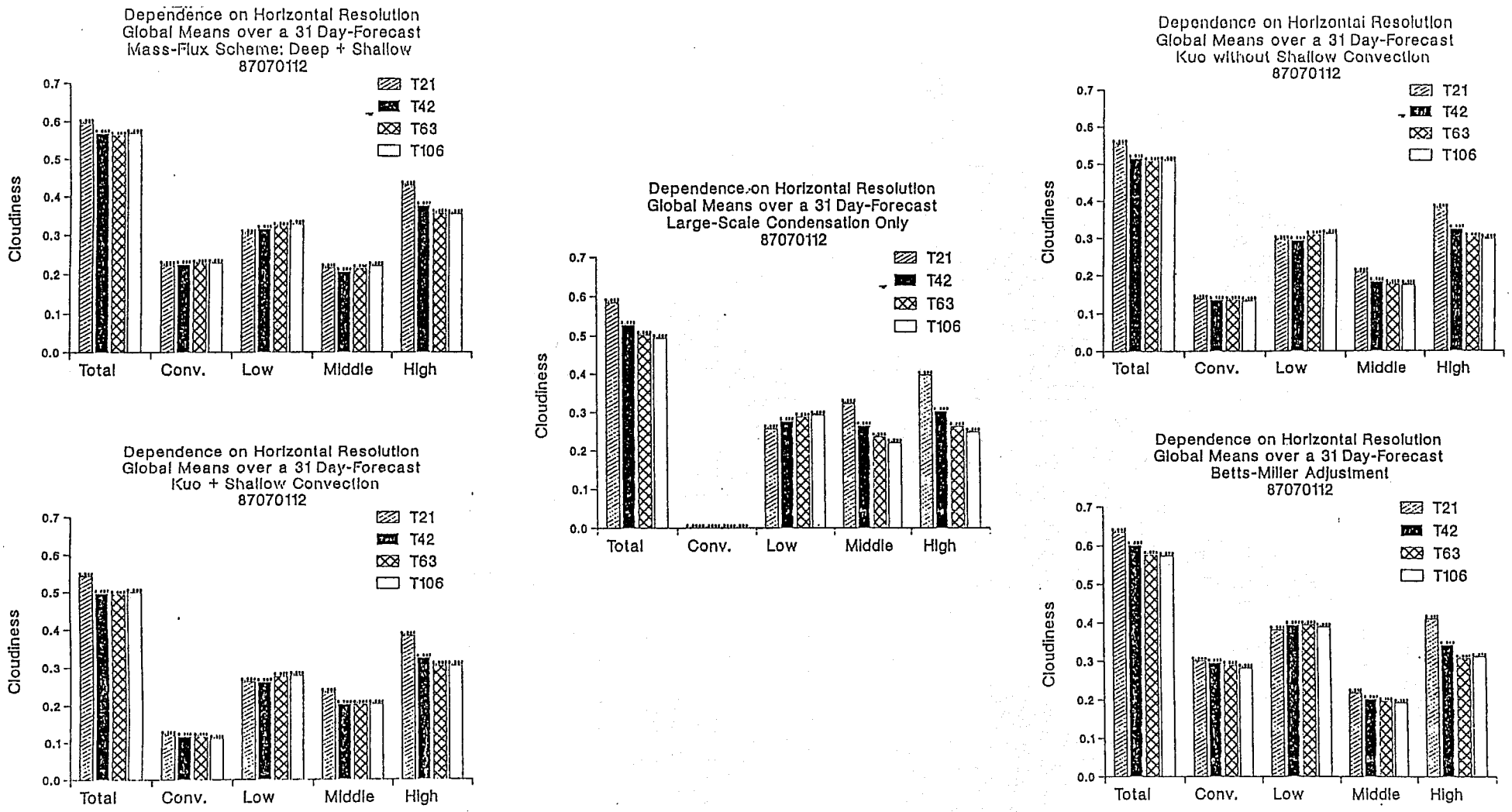

Fig. 28 The different components of the globally averaged cloudiness at four horizontal resolutions (T21, T42, T63 and T106) in simulations performed with different parametrizations of the moist processes.

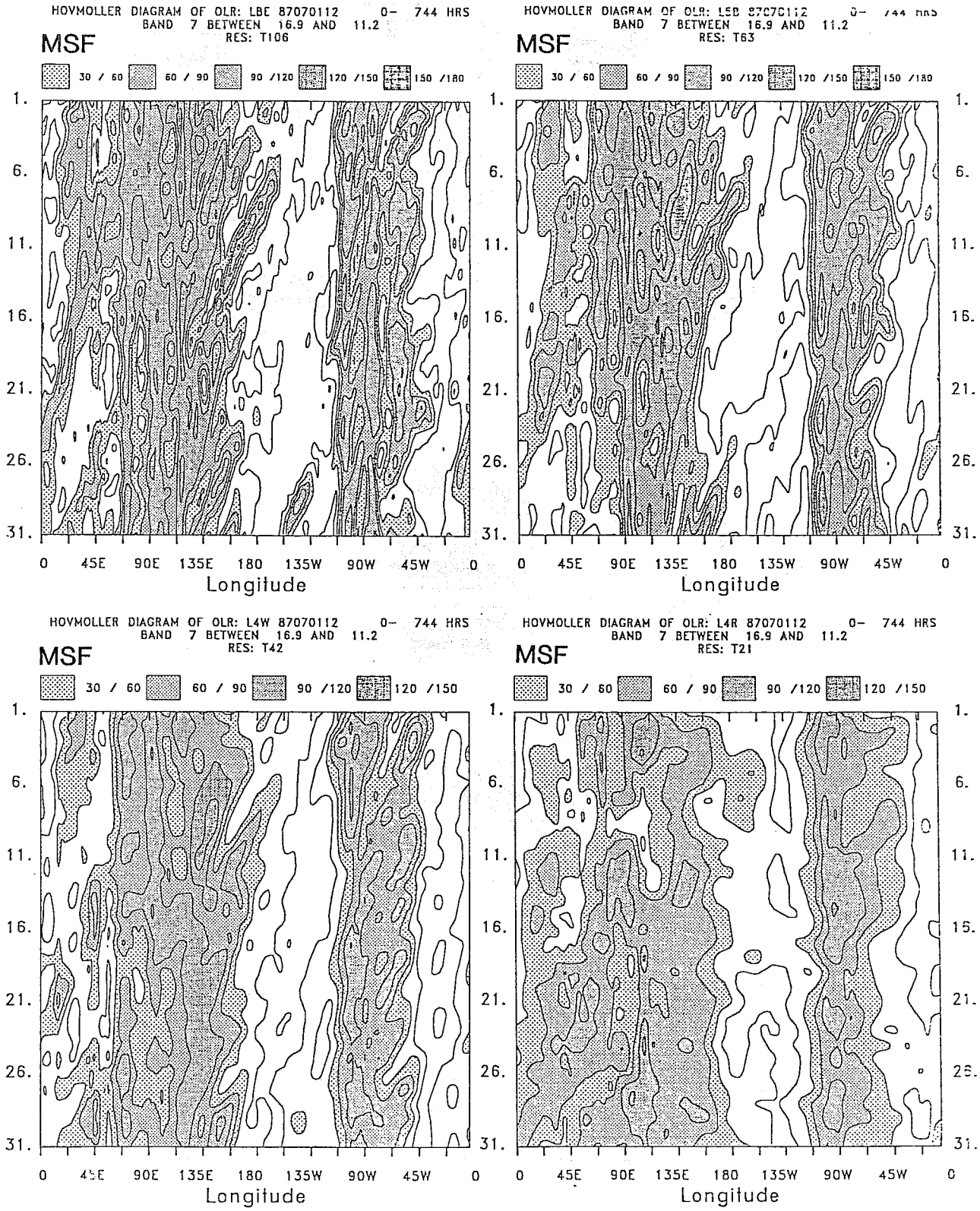

Fig. 29 The Hovmöller diagram of the cloud longwave forcing during July 1987 as simulated by the cycle 36 version of the ECMWF at four horizontal resolutions. Model radiative fluxes are processed over the latitude band 16.9-11.2°N.

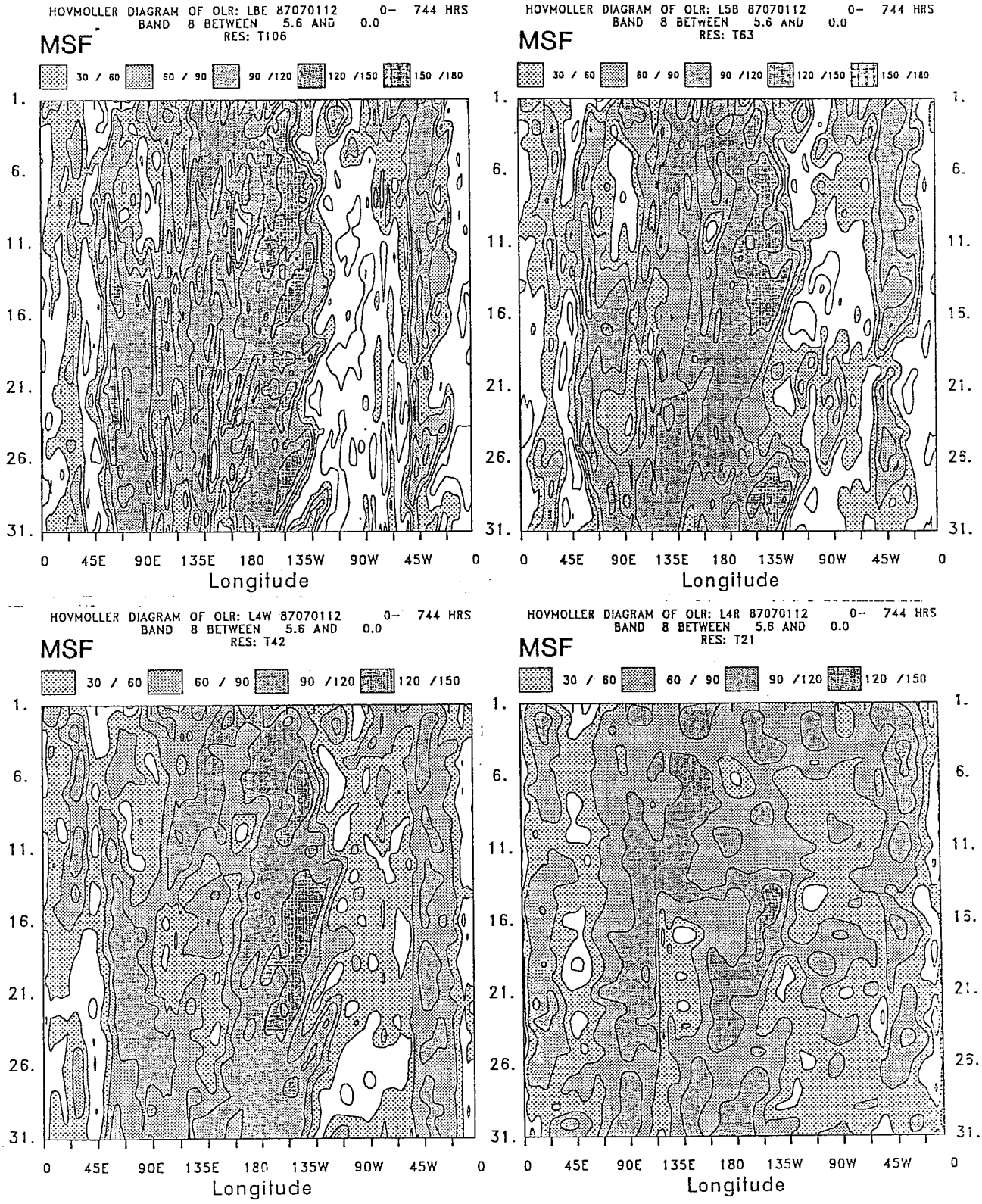

Fig. 30 As in Fig. 29, but for the latitude band 5.6- 0°N.

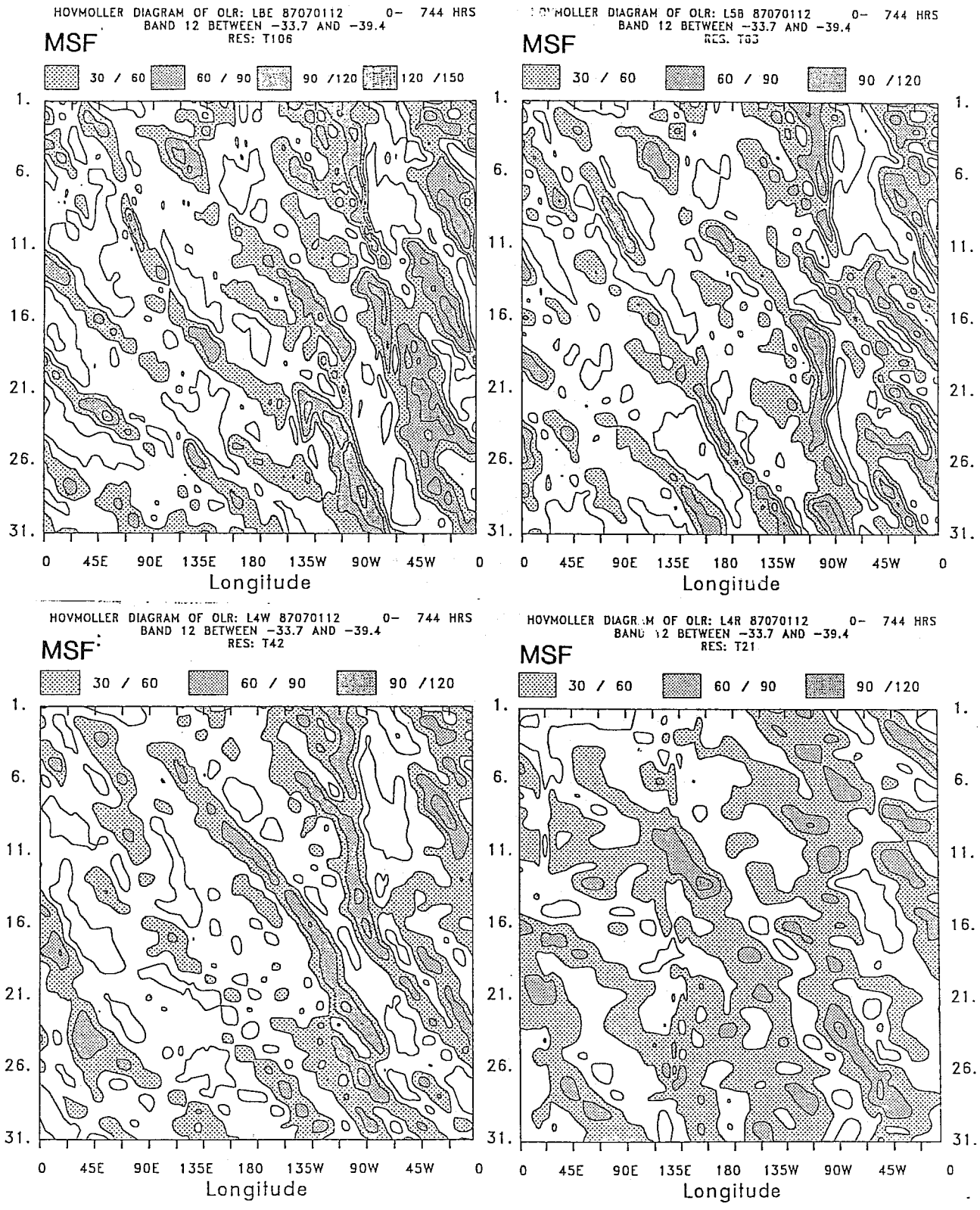

Fig. 31 As in Fig. 29, but for the latitude band 33.7-39.4°S.